



HAL
open science

Hydrogeochemical processes of critical zone developed in Tégulines Clay, Paris Basin: Hydrogeochemical and multi-isotopic approach ($\delta^{13}\text{C}$, δD , $\delta^{18}\text{O}$, $^{87}\text{Sr}/^{86}\text{Sr}$ and ^{14}C)

Catherine Lerouge, Mathieu Debure, Ana-Maria Fernández, Philippe Négrel, Benoit Madé, Nicolas Maubec, Christine Fléhoc, Catherine Guerrot, Michaela Blessing, Benoit Henry, et al.

► To cite this version:

Catherine Lerouge, Mathieu Debure, Ana-Maria Fernández, Philippe Négrel, Benoit Madé, et al.. Hydrogeochemical processes of critical zone developed in Tégulines Clay, Paris Basin: Hydrogeochemical and multi-isotopic approach ($\delta^{13}\text{C}$, δD , $\delta^{18}\text{O}$, $^{87}\text{Sr}/^{86}\text{Sr}$ and ^{14}C). *Journal of Hydrology*, 2023, 617, pp.129077. 10.1016/j.jhydrol.2023.129077 . hal-03948630

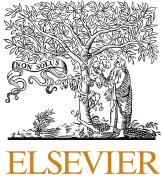
HAL Id: hal-03948630

<https://brgm.hal.science/hal-03948630>

Submitted on 31 May 2023

HAL is a multi-disciplinary open access archive for the deposit and dissemination of scientific research documents, whether they are published or not. The documents may come from teaching and research institutions in France or abroad, or from public or private research centers.

L'archive ouverte pluridisciplinaire **HAL**, est destinée au dépôt et à la diffusion de documents scientifiques de niveau recherche, publiés ou non, émanant des établissements d'enseignement et de recherche français ou étrangers, des laboratoires publics ou privés.



Research papers

Hydrogeochemical processes of critical zone developed in Tégulines Clay, Paris Basin: Hydrogeochemical and multi-isotopic approach ($\delta^{13}\text{C}$, δD , $\delta^{18}\text{O}$, $^{87}\text{Sr}/^{86}\text{Sr}$ and ^{14}C)

Catherine Lerouge^{a,*}, Mathieu Debure^a, Ana-Maria Fernandez^b, Philippe Négrel^a, Benoit Madé^c, Nicolas Maubec^a, Christine Fléhoc^a, Catherine Guerrot^a, Michaela Blessing^a, Benoit Henry^a, Jean-Charles Robinet^c

^a BRGM, 45060 Orléans, France

^b CIEMAT, Departamento de Medio Ambiente, 28040 Madrid, Spain

^c ANDRA, 1-7 rue Jean-Monnet, 92298 Châtenay-Malabry Cedex, France

ARTICLE INFO

Keywords:

Tégulines Clay
Critical zone
Landscape
Water transfer
Hydrogeochemistry
Multi-isotopic approach

ABSTRACT

Water transfers and processes governing the chemistry of groundwaters and clay pore waters were investigated in the critical zone developed in Tégulines Clay in the area of Brienne-Le-chateau, at east of the Aube alluvium plain (France). A pit-digging campaign along two-stepped west-facing hillslopes along the Brevonne valley and the Aube/Brevonne paleo-valley gives evidence of a thin Quaternary clay silty and carbonate-free loams overlying Tégulines Clay, mobile regolith along the slopes and the presence a carbonate alluvium layer in pits of the Brevonne valley. Groundwaters at the first ridgetop attest of a temporary perched water table, while groundwaters at top of Tégulines Clay along the first west-facing steep slope toward the Brevonne River provide evidence of lateral groundwater transfers and runoff of waters toward the valley which is a discharge zone belonging to the present-day Aube alluvium plain. Groundwaters have low concentrations of Total Dissolved Solids (TDS < 600 mg/L) and are calcic-carbonate waters. Their $\delta^{18}\text{O}$ and δD of groundwaters are consistent with local meteoric values. An ^{18}O and D enrichment in groundwaters at the bottom of the second hillslope and in waters from reservoirs indicates evaporation processes. The $\delta^{13}\text{C}_{\text{CO}_2}$ of dissolved inorganic carbonate in groundwaters is essentially due to degradation of organic matter. The composition of the pore waters from Tégulines Clay in boreholes are chemically heterogeneous and different from groundwaters. They are Ca-Mg-SO₄-rich and show a large range of TDS concentrations (592–6457 mg/L). The highest values are measured in the most intensely weathered clay developed in the first 10–15 m under the first ridge top and the low east-facing slope of the Aube/Brevonne paleo-valley. This latter seems to represent a large intermediate discharge zone between the coarse ridgetops (recharge zones) and the current Aube alluvium plain. The $\delta^{18}\text{O}$ and δD of pore waters are aligned along the local meteoric water line, indicating that meteoric waters have diffused through the clay formation during post-depositional history and replaced original connate seawater. On contrary the $^{87}\text{Sr}/^{86}\text{Sr}$ ratios of pore waters remain almost similar to that of Lower Cretaceous seawater, suggesting a limited diffusion of Sr since the formation deposition. Toward the top of the formation in the Aube/Brevonne paleovalley, major cation and anion concentrations, ^{18}O and D enrichment and a slight increase of the $^{87}\text{Sr}/^{86}\text{Sr}$ ratios suggest the diffusion of evaporated waters. The $\delta^{13}\text{C}$, $\delta^{18}\text{O}$, $^{87}\text{Sr}/^{86}\text{Sr}$ ratios and ^{14}C activity of concretions at top of Tégulines Clay show that they precipitated from evaporated old groundwaters one at ~ 34 ky in the TPH2-1 pit at the ridgetop of the second hillslope and a younger age of ~ 8 ky in the TV4-1 pit.

* Corresponding author.

E-mail address: c.lerouge@brgm.fr (C. Lerouge).

<https://doi.org/10.1016/j.jhydrol.2023.129077>

Received 14 October 2022; Received in revised form 8 December 2022; Accepted 3 January 2023

0022-1694/© 20XX

1. Introduction

The understanding of solute transport in critical zone (CZ) developed in clay formation is an issue of primary importance both for the preservation of our natural environment and more specifically for long-term assessment of the efficiency of the sub-surface geological waste repository. Clay formations effectively act as a natural low-permeability protective barrier preventing contamination of groundwater resources due to extremely long time scales for groundwater flow and solute transport, and to the capacity of clay minerals to fix cationic and oxyanionic toxic chemicals (Debure et al., 2018, 2020; Desaulniers et al., 1981; Gaucher et al., 2006; Hendry et al., 2004; Hendry and Wassenaar, 2000; Mazurek et al., 2011; Mazurek et al., 2009; Remenda et al., 1994).

The study of the critical zone requires specific investigations of earth-surface processes and water and solute transfers crossing time scales, from geological times to “anthropic time”. To cross such scales need to analyse present-day waters and the records of the water fluxes in the geologic media (e.g., soils and sediments) with time. Interactions in CZ between the marine reduced clay formation and surficial reservoirs including the atmosphere that is an infinite oxygen reservoir, the hydrosphere and vegetation induce mineral, chemical, petrophysical and mechanical changes in the clay formation, that influence pore water chemistry and solute transfers (Bolton et al., 2006; Brantley et al., 2013; Hendry and Wassenaar, 2000; Jin and Brantley, 2011; Jin et al., 2013; Jin et al., 2010; Lerouge et al., 2018; Sullivan et al., 2016; Tremosa et al., 2020; Tuttle and Breit, 2009; Tuttle et al., 2009). The reaction rates in the CZ are the highest in the vadose zone and especially in the zone where the water table varies. Indeed, the water slows the O₂ migration rate since the diffusion of gases is faster in the air than in water. In this zone, complex and overlapping biogeochemical reactions occur that require reactive transport modelling to be deconvoluted and reconciled (Li et al., 2017; MacQuarrie and Mayer, 2005). Discrepancies are frequently observed when trying to extrapolate laboratory data used for modelling at the field scale (Guo et al., 2020; Tremosa et al., 2020; Maher et al., 2006; Pacheco and Alençon, 2006). Often, either field data used as input of the models are acquired in constrained environments or modelling of the field is restricted to some specific area of interest (Bao et al., 2017; Milesi, 2020; Li et al., 2014). Such models remain often one-dimensional models, conceptual models or focus only on a little part of the investigated watershed (one borehole or several trenches of a few dozen of centimetres) or on the major biogeochemical reactions (Bao et al., 2017; Milesi, 2020; Li et al., 2014; Arizaleta, 2020; Mayer et al., 2015). An important aspect of assessing the long-term efficiency of the near-surface repository is developing a comprehensive understanding of the hydrogeochemical functioning of the entire targeted area in the watershed, in order to define initial conditions of the disposal and to predict water flows. For this reason, it remains essential to obtain the most complete dataset (mineralogy, geochemistry, petrophysical properties, and hydrogeology).

For a decade, Tégulines Clay, a low-permeability clay formation outcropping in the area of Brienne-le-Chateau (north-eastern France) has been investigated in the context of surface repository for low-level radioactive waste by ANDRA (the French National Radioactive Waste Management Agency). A multi-disciplinary approach has been applied to core samples from boreholes of three successive drilling campaigns through the clay formation to define the depth of the critical zone and the key parameters controlling chemistry of Tégulines Clay pore waters. A detailed petrological study based on major iron-bearing redox-sensitive minerals (FeII: pyrite, siderite, ankerite, clay minerals) and on the valence of iron combined with the petrophysical properties allowed defining the depth of the CZ in the AUB1010 borehole and proposing a first sketch model of the redox changes in the Tégulines Clay (Lerouge et al., 2018). Oxidation in Tégulines Clay is characterized more by progressive reactions than by a sharp redox reaction front. The oxidation

reactions extend down to ~20 m, depth corresponding to the transition between a nonplastic to a plastic rock and the oxidation of diagenetic glauconite pellets. A complementary gas monitoring (CO₂, O₂, N₂, alkanes) on core samples of Tégulines Clay from AUB1010, AUB230 and AUB240 boreholes, and carbon isotopes on CO₂ allowed defining the consequences of weathering processes on gases dissolved in pore waters (Lerouge et al., 2020). The dataset showed that the first < 10–12 m zone of Tégulines Clay corresponds to a highly reactive clay influenced essentially by pyrite oxidation, calcite dissolution and degradation of organic matter, and formation of iron-hydroxides (Le meur et al., 2021). The δ¹³C of CO₂ indicates that organic matter degradation was a major source of CO₂ at shallow depths and down to 10–12 m, which is the maximum depth at which we observed fossil roots. All these data constituted a first set of parameters for the building of a 1D vertical solute reactive transport modelling through the Tégulines Clay (Lerouge et al., 2018; 2020). However, hydrogeochemical processes remain poorly constrained in the studied area.

The main objectives of this work were to further investigate hydrogeochemical processes of CZ developed in Tégulines clay in the studied area, based on hydrogeochemistry combined with a multi-isotopic approach (δ¹³C, δD, δ¹⁸O, ⁸⁷Sr/⁸⁶Sr and ¹⁴C). Such approach has been developed at Susquehanna Shale Hills CZ Observatory (Sullivan et al., 2016, and references therein). The new field campaign at east of Brienne Le Chateau and Juzanvigny included boreholes and pits dug along two-stepped west-facing hillslopes corresponding to the Brevonne valley and the Aube/Brevonne paleo-valley, on the eastern side of the Aube alluvium plain. The campaign of pit digging aimed at examining the conversion of Tégulines Clay into regolith and overlying sediments and soils, the root network, downslope transport of mobile regolith, and at sampling waters (rainfall, surficial reservoirs and groundwaters). Additional deep boreholes (30 to 90 m) allowed sampling Tégulines Clay through the CZ and below, in order to 1) define the variability of depth of the weathering profile in the studied area, and 2) obtain Tégulines Clay pore waters for hydrochemistry. Chemical analyses of pore waters in claystones is challenging. It can be obtained either by squeezing of samples (Fernandez et al., 2014) or by chemical pore water modelling using Phreeqc (Gaucher et al., 2009; Wersin et al., 2016). First chemical analyses of Tégulines Clay pore waters by squeezing are available in Lerouge et al. (2018, 2020). In this paper, we completed the dataset by pore water chemical data calculated with the Phreeqc model of Gaucher et al. (2009) and already developed for Tégulines Clay in Lerouge et al. (2020). The Pore water chemical model is based on anion leaching (Cl⁻, SO₄²⁻ and NO₃⁻), measurement of exchangeable cations using the method described in Hadi et al. (2016), the dissolved inorganic carbon (DIC) obtained by core degassing (Girard et al., 2005; Lerouge et al., 2020), and mineral assemblage (Lerouge et al. 2018). Hydrogeochemistry of waters allowed characterizing the hydrochemical facies and mechanisms controlling water chemistry, including water–rock interactions, dilution and evaporation processes (Cherchali et al., 2020; Li et al., 2013). Here we examined more specifically the role of the clay interlayers as cation exchanger, according to Cloutier et al. (2008). The multi-isotopic (δ¹³C, δD, δ¹⁸O, ⁸⁷Sr/⁸⁶Sr and ¹⁴C) approach was applied on waters to elucidate their origin and their age (Ferguson et al., 2020; Sullivan et al., 2016). A similar multi-isotopic (δ¹³C, δ¹⁸O, ⁸⁷Sr/⁸⁶Sr and ¹⁴C) approach was carried out on carbonate concretions which recorded episodes of the high reactivity of Tégulines Clay at the top of the formation.

2. Geological setting and field campaign

The studied area is located in the area of Brienne Le Chateau and Juzanvigny, in the eastern part of the Paris Basin (Fig. 1a). The Brienne Plain is bounded to the north by the Chalky hills of the Cenomanian (100.5 Ma to 93.9 My) from which flows the Voire River, a tributary of the Aube River, and to the west and the south by hills carved by the

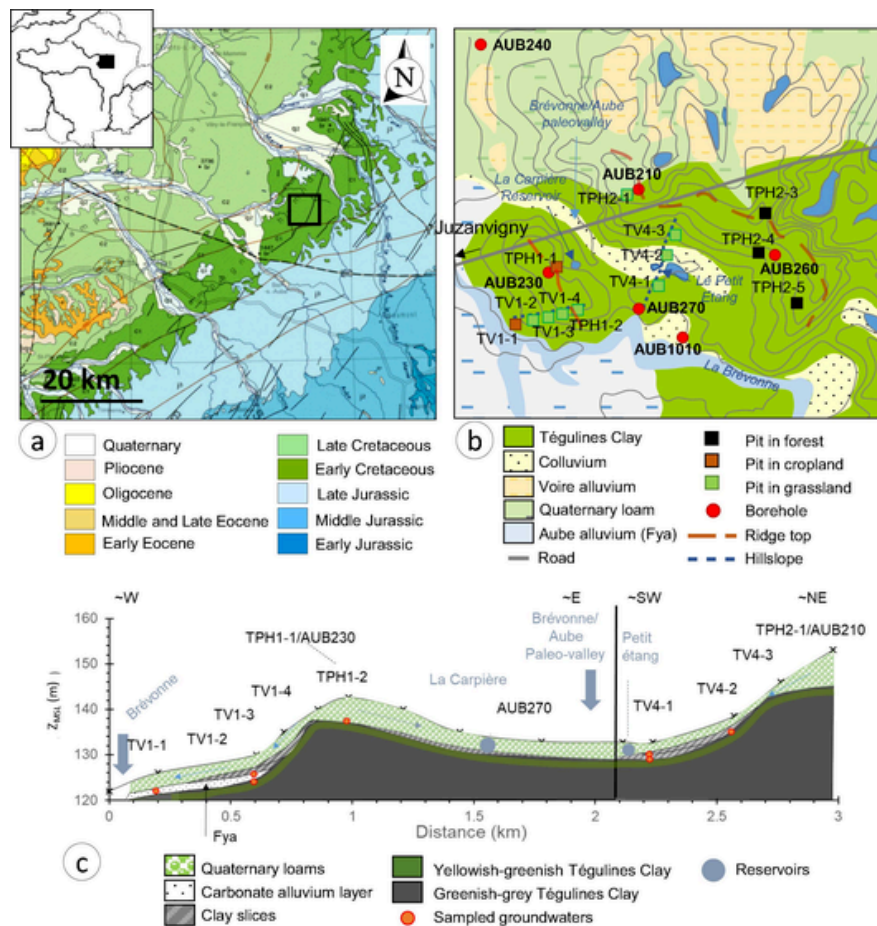


Fig. 1. (a) Geological map of the eastern part of the Paris basin and location of the studied area; (b) Geological map of the studied area with topology and location of boreholes and pits; (c) Cross-section along the two stepped fluvial terraces, showing the lithology and the of reservoirs, pits and boreholes and groundwaters occurrences in pits. Z_{MSL} is the altitude given in meters above mean sea level.

Aube river in the Tégulines Clay of Early Cretaceous age (145 to 100.5 My) (Voinchet et al., 2015). The Aube River deposited five stepped fluvial terraces in the alluvial plain of Brienne in relation to the major climatic cycles throughout the Middle Pleistocene (780 000 to 125 000 yr; Hatrival et Menillet, 2002; Voinchet et al., 2015). Currently, smooth reliefs characterize the area of Brienne-Juzanvigny. The distribution of the residual flaps of the five-stepped fluvial deposits indicates that the present-day Aube river flowing in the middle of the plain has flowed far away in the past (Voinchet et al., 2015).

The main hydrologic reservoir of the region is a vast cone of sedimentation which filled the Aube Valley and forms a wide alluvial plain passing between Brienne-le-Château and Juzanvigny (Hatrival and Menillet, 2002). Sediments consist of calcareous sands and gravels whose thickness increases from upstream to downstream, and are covered by loams. The Tégulines Clay forms the low-permeability substratum of this reservoir. The Aptian Greensands underlying Tégulines Clay and Overlying Plicatules Clay form a captive aquifer (Hatrival and Menillet, 2002). The large lakes of the reservoir dams of the Paris city (“Seine” and “Aube” reservoirs) are located in the southeast of the study area (Fig. 14a). Thirteen ~ 5 m deep pits were dug, and five boreholes were drilled in the area of Juzanvigny, to have a better knowledge of the distribution of the Quaternary formations and the weathering profile depths in the Tégulines Clay in studied area (Fig. 1b). Pits were dug in October 2017 along two ridgetops (dotted red lines) and associated hillslopes (dotted blue lines) on the eastern side of the present-day Aube River valley (Fig. 1b and 1c). Eight pits were dug in grasslands (green squares), two in croplands (orange squares) and three in forest (black

squares). Drainage has been installed in the 1980 s at about 1 m depth in cropland in which the TPH1-1 pit and AUB230 borehole were drilled. During digging, some groundwaters flowed in the pits. Those waters were especially abundant in two pits located at the bottom of the first hillslope (TV1-1 and TV1-2) where an alluvium layer released plenty of water which flooded the pits more than a meter high (Fig. 2).

Two boreholes (AUB210, AUB230) entirely crosscut the three units of the Tégulines clay formation (an upper carbonate-clay rich unit, a clay-rich unit, and a clay-quartz rich unit) (Lerouge et al., 2018). The AUB240 borehole drilled at the north of Juzanvigny in May 2018 crosscut several meters of Brienne marls before crosscutting ~ 70 m of Tégulines Clay without reaching the Aptian Greensands. This borehole is considered as the reference borehole for mineralogy, physical and chemical properties of Tégulines Clay due to the overlying Brienne marls that protect them from weathering. The AUB230 borehole, drilled in place of the TPH1-1 pit on the first ridgetop in December 2017, entirely crosscut ~ 63 m of Tégulines Clay before attaining Greensands at 68 m. The AUB210 borehole, drilled in place of the TPH2-1 pit on the second ridgetop in October 2018, crosscut ~ 76 m of Tégulines Clay before attaining Greensands at ~ 84 m. The AUB260 and AUB270 boreholes drilled in October 2018 are two 30 m-deep boreholes crosscutting the weathering zone of Tégulines Clay. AUB260 is near the TPH2-4 pit on the second ridgetop, whereas AUB270 is near the TV4-1 pit at the bottom of the second hillslope, corresponding to the paleo-valley of Brevonne/Aube River.

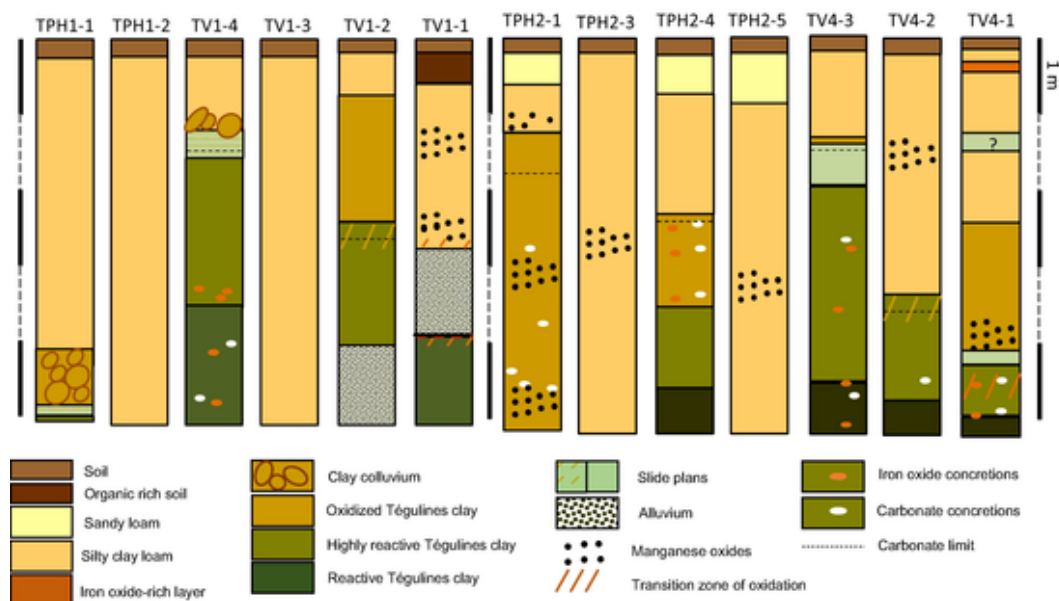


Fig. 2. Lithological log of the thirteen pits along the two stepped fluvial terraces.

3. Sampling and methods

The soil, sediment and rock samples were regularly taken at least every meter in 5-m deep pits. In boreholes they were taken every meter down to 15 m, then every-five meters down to 30 m, and every ten meters below 30 m in boreholes (Fig. 4). The samples were rapidly and systematically conditioned on the field to limit the atmospheric contact. Two types of conditioning were used:

- 1) Aluminum bags sealed under vacuum for mineralogy, water content, chemical and isotopic analyses;
- 2) Glass jars under He pressure of 700 mbars for gas monitoring and concentration (DIC) and isotopic composition of CO_2 dissolved in pore waters.

Groundwaters flowing from the pit wall were directly collected in small vials; vials were systematically filled to limit atmospheric contact and maintained at temperature of $\sim 4^\circ\text{C}$.

Two reservoirs and rainfall were also sampled.

A multidisciplinary approach was applied to water samples and rock samples. Water analyses included a measure of pH, alkalinity, major anions and cation concentrations, their $\delta^{18}\text{O}$ and δD , and ^{14}C to approximate their age. Rock characterization included petrology, mineral quantification, anion leaching, cation exchange capacity, sample degassing to estimate DIC and measurement of $^{87}\text{Sr}/^{86}\text{Sr}$ ratio of exchangeable strontium. Calcite concretions were analysed for their $\delta^{13}\text{C}$, $\delta^{18}\text{O}$, and $^{87}\text{Sr}/^{86}\text{Sr}$ ratio, in order to determine their origin, and for ^{14}C , in order to estimate their age. The details of the collecting procedure, sample preservation from oxidation are extensively described in former papers (Lerouge et al., 2018; 2020). Analytical techniques are given in the [supplementary file SD1](#).

4. Results

4.1. Field observations

4.1.1. Hillslopes

The two hillslopes correspond from west to east to the present-day west-facing hillslope of the Brevonne River and the old west-facing hillslope of the Aube/Brevonne River (Fig. 1c). The Aube old valley is characterized by near-planar slopes that are topographically asymmetric,

with slightly steeper ($\sim 4\%$) west-facing than east-facing ($\sim 2\%$) hillslopes. The east-facing hillslopes are mantled with more variable regolith than the west-facing hillslopes.

Tégulines Clay generally does not directly outcrop. Observations of the thirteen 5 m-deep pits show that Tégulines Clay are covered by Quaternary sediments then ~ 30 cm-thick soil (Fig. 2). The thickness of Quaternary sediments varies from < 1 m up to more than 5 m in the pits TPH1-2, TV1-3, TPH2-3 and TPH2-5, where Tégulines Clay are not reached (Fig. 2). Along both hillslopes, Quaternary sediments mainly consist of yellowish silty clay loam with a few occurrences of overlying beige sandy loam (< 1 m-thick) at the top of the second hillslope (pits TPH2-1, TPH2-4 and TPH2-5) (Fig. 2). Silty clay loam is relatively sticky and characterized by manganese oxides-rich levels present at different depths, and by a greyish network particularly developed in the first meters in association with the system of living roots, but also dead roots (Fig. 2). The silty clay loam directly overlies Tégulines Clay, except in the TV1-1 and TV1-2 pits in the valley of the Brevonne River, where a carbonate alluvium layer overlies in-place green and slightly decompacted Tégulines Clay. That provides evidence of an erosion phase followed by the alluvium deposit in the valley. In the TV1-2 pit, the alluvium layer separates a ~ 3 m-thick slice of weathered Tégulines Clay from the in-place Tégulines Clay. These two pits provide evidence of an erosion phase followed by the alluvium deposit in the valley, and of local sliding of clays along the slope later than carbonate alluvium deposit.

The top of Tégulines Clay corresponds to a change of colour from yellow to light green-yellow (Fig. 3b, d), the presence of calcite (further noted calcite transition) (Fig. 3g), and in some cases to slip surfaces (TPH1-1, TV1-4, TV4-3 and TV4-1; Fig. 3c). A layer of clay colluvium covers Tégulines Clay in place in the TPH1-1 and TV1-4 pits (Fig. 2; Fig. 3d). Yellow Tégulines Clay corresponds to oxidized facies containing some manganese oxides-rich levels (Fig. 3f) and iron hydroxides (Fig. 3j). The thickness of yellow Tégulines Clay attains 4 m in the TPH2-1 pit at the top of the second hillslope, and 1–2 m at the bottom of the two hillslopes (TV1-1 and TV4-1 pits). Calcite is present as secondary cm-sized concretions or a thin white calcite layer (Fig. 3; Fig. 3g, i). The root network that crosscut Quaternary sediments also crosscut Tégulines Clay down to 5 m depth (Fig. 3e).

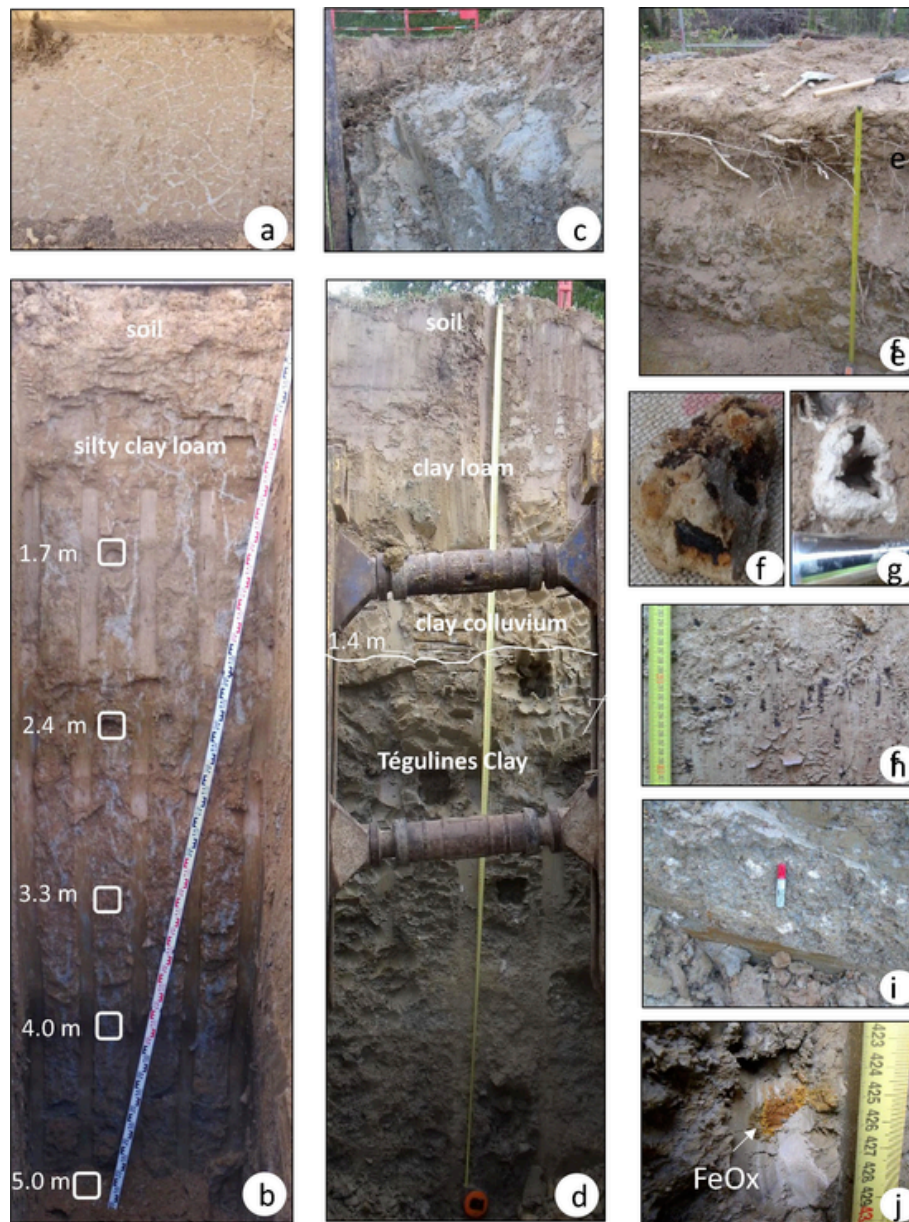


Fig. 3. (a) Bottom of the soil pit; (b) TPH1-1 pit through ~ 5 m-thick yellowish silty clay loam crosscut by a root network marked by a grey colour; (c) Excavation of the TV4-3 pit showing yellow clay loam overlying grey greenish Tégulines Clay; the top of the clay formation is marked by a slide surface; (d) TV4-3 pit showing the lithological transition between surficial formations and Tégulines Clay; (e) sandy loam observed in the TPH2-3 soil pit; (f) Manganese oxides; (g) Carbonate concretions in the TPH2-1 pit; (h) layer of nodules of manganese oxides at 2.9 m depth in the TPH2-1 pit; (i) Carbonate concretions at the top of Tégulines Clay in the TV4-3 pit (detail of the c image); (j) Iron hydroxides (FeOx) at 4.25 m depth in the TV4-3 pit. (For interpretation of the references to colour in this figure legend, the reader is referred to the web version of this article.)

4.1.2. Boreholes

The AUB240 reference borehole crosscut several meters of alluvium before attaining the Brienne marls at 8.4 m and the Tégulines Clay at ~ 20 m (Fig. 4). Tégulines Clay crosscut by this borehole is compact and dark green and has a homogeneous aspect. The bottom of Tégulines Clay is not attained in this borehole.

The AUB210 borehole drilled near the TPH2-1 pit crosscut ~ 1 m of quartz sandy loam, then ~ 7–8 m of yellow silty clay loam before attaining the top of Tégulines Clay (Fig. 4). Very rapidly, the Tégulines Clay changes from ochrous to yellowish-greenish colour until ~ 14 m and to greenish-grey until ~ 18 m. Below 18 m clay is compact and dark green. The last ten meters are very dark green, and richer in glauconite and silty quartz.

The AUB230 drilled near the TPH1-1 pit crosscut ~ 30 cm of brown soil, ~5 m of yellow silty clay loam before attaining the top of Tégulines Clay, marked by plastic texture and ochrous colour (Fig. 4). Tégulines Clay changes rapidly from ochrous to yellowish-greenish colour until ~ 11 m and to greenish-grey until ~ 20–25 m. Below 20–25 m clay is compact and dark green. The last few meters are very dark green, richer in glauconite and silty quartz. The bottom is marked by the presence of phosphates.

The AUB260 borehole drilled near the TPH2-4 pit crosscut ~ 30 cm of light brown soil, ~60 cm of quartz sandy loam, then ~ 5.3 m of yellow silty clay loam before attaining the top of Tégulines Clay (Fig. 4). Tégulines Clay is ochrous and plastic until 7–8 m, and changes progressively from ochrous to yellowish-greenish colour until ~ 10–11 m, and to greenish-grey until ~ 13–14 m. Some roots are observed down to

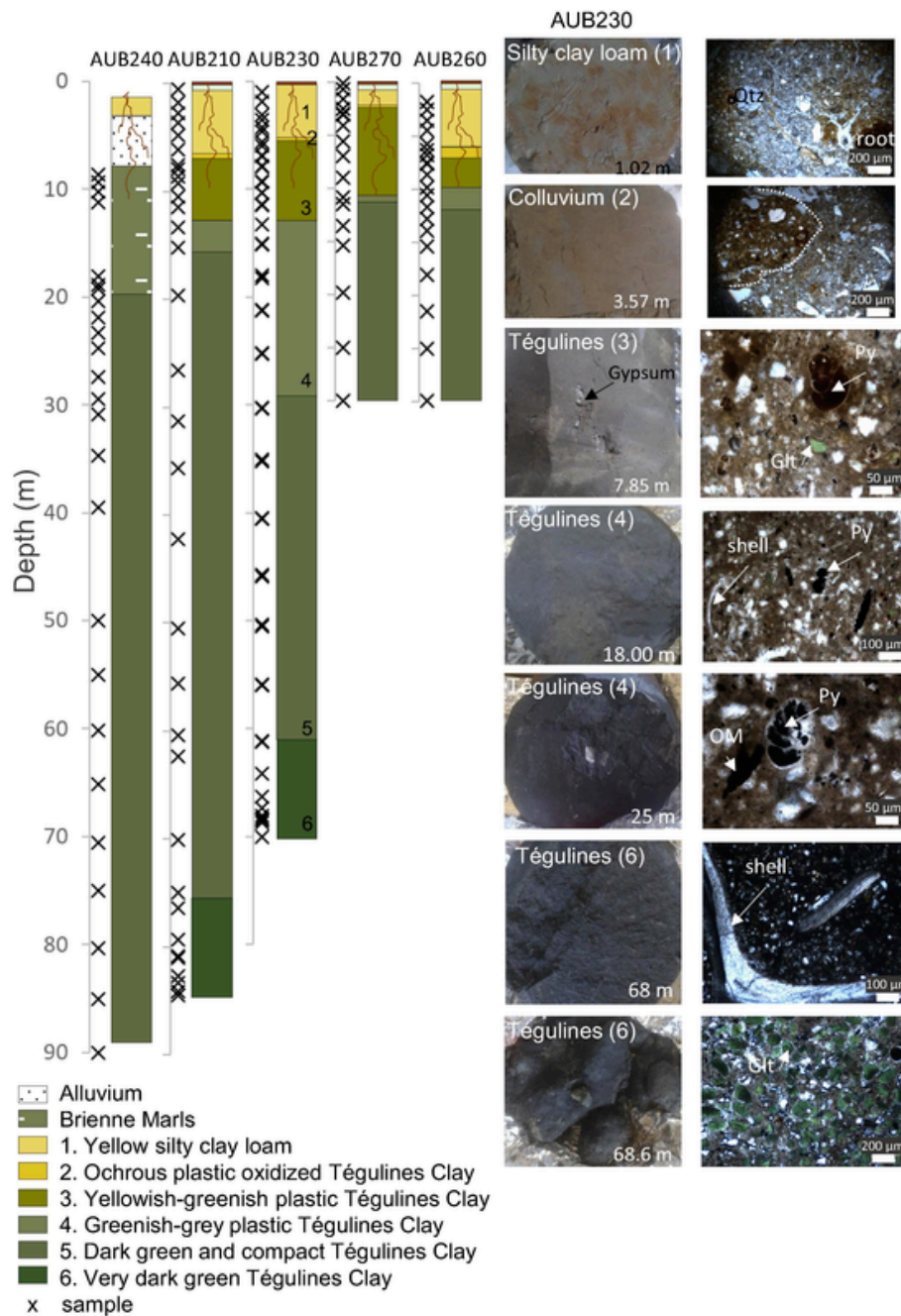


Fig. 4. Descriptive lithological log of the five boreholes of the 2018 drilling campaign and sampling (cross). On the right side, macroscopic view and microscopic micrograph of samples characteristic of the different zones of the weathering profile in Tégulines Clay from the AUB230 borehole. Abbreviations: Glt, glauconite; Py, pyrite; OM, organic matter.

10 m depth. Below ~ 13–14 m clay is compact and has a dark green colour. Between 20 and 30 m, it is rich in carbonate bioclasts, pyrite and phosphates.

The AUB270 borehole drilled near the TV4-1 pit crosscut ~ 30 cm of light brown soil, ~60 cm of quartz sandy loam, then ~ 2 m of yellow silty clay loam before attaining the top of Tégulines Clay (Fig. 4). Clay is ochrous, plastic and contains carbonate concretions in the first 20 cm, and rapidly changes from ochrous to yellowish-greenish colour at ~ 3 m until ~ 11 m, and to greenish-grey and rapidly to dark green. A small root is observed at 10.8 m. Between 12 and 30 m, Tégulines Clay is rich in carbonate bioclasts.

The different zones identified in the weathering profile of the Tégulines clay formation crosscut by the different AUB210, 230, 260 and

270 boreholes are almost similar, but their thickness varies from one borehole to another (Fig. 4). The yellowish-greenish plastic reactive zone, characterized by the intense oxidation of pyrite, and the presence of iron hydroxides and gypsum, is the thickest in AUB230 and AUB270 boreholes. The greenish-grey plastic zone is the thickest in the AUB230 borehole and is limited to few meters in other boreholes. Below, Tégulines Clay is compact and seems to be preserved from oxidation.

5. Sediment characterization

5.0.1. Surficial formations

It was sometimes difficult to make clear limits between yellow silty loam, colluvium and top of Tégulines Clay on the field (Fig. 3d). The mineralogy of surficial formations and Tégulines Clay was characterized in details in the TPH1-1 pit and associated AUB230 borehole.

Yellow silty clay loam of the TPH1-1 analysed by XRD consist of ~ 61–70 wt% of quartz and 21–32 wt% of clay minerals with minor plagioclase, K-feldspar and rutile. The clay fraction characterized by < 2 µm XRD consists of kaolinite (31–39 wt%), smectite-rich illite-smectite mixed layers (40–51 wt%), illite-mica (18–21 wt%) and traces of chlorite-vermiculite.

In thin sections, quartz essentially occurs as numerous < 60 µm detrital grains and coarse grains (100–400 µm; Fig. 4). The amount of coarse quartz grains varies from one pit to another. Clay mineral fraction occurs as a yellow-brownish fine disseminated matrix but also as brownish altered glauconite pellets resulting from Tégulines Clay and possibly Greensands dismantling. Colluvium is free of coarse quartz grains and is an agglomerate of Tégulines Clay roundish blocks showing various states of alteration and impregnation by iron hydroxides. In all the pits, some layers contain Mn oxides or are rich in iron hydroxides that are not detected by XRD analyses.

Infrared spectra on all the samples show that carbonates are absent from the surficial formations and revealed only the presence of quartz, clays and iron oxyhydroxides such as goethite. The carbonate's absence was used as a tracer to determine the depth of the surficial formations. The top of the Tégulines Clay is reached once the carbonates were detected.

5.0.2. Tégulines Clay

The top of Tégulines Clay attained at about 5 m below the ground surface, consists of plastic entirely oxidized claystone (57 wt% of clay and 42 wt% of quartz-feldspar), with a brown network associated with roots. XRD does not detect carbonates, but they still occur as rare residual calcite bioclasts. Gypsum and iron hydroxides entirely replaced pyrite nodules and frambooids. The clay fraction is highly rich in smectite-rich illite-smectite mixed layers (77–84 wt%) with kaolinite (14 wt%) and minor illite-micas (2–3 wt%) as illustrated in Fig. 5.

Below 5 m, the XRD quantification allows dividing the clay formation into three parts:

- (1) a carbonate-clay rich unit, between 5 and 25 m, characterized by an increase of the calcite content from 16 to 27 wt% toward the surface, and by the lowest quartz – feldspar silty contents (20–31 wt%).
- (2) a clay-rich unit, between 25 and 55 m, characterized by the highest clay content (50–53 wt%), 4–8 wt% of carbonates and lower quartz-feldspar silty content (32–41 wt%).
- (3) a clay-quartz-rich unit, between 55 and 67 m, characterized by high quartz – feldspar silty content (39–44 wt%) and low carbonate contents of 4–9 wt%.

Between 5 and 11 m, Tégulines Clay is yellowish-greenish, and highly reactive; all the Fe-bearing minerals, including pyrite, glauconite are partially oxidized, calcite gives evidence of partial dissolution, while gypsum and goethite precipitate. Clay fraction approximatively consists of mixing between kaolinite (34–37 wt%), illite-smectite mixed layers (38–43 wt%), illite-micas including glauconite (22–25 wt%) with traces of chlorite (< 1 wt%) as illustrated in Fig. 5.

Down to a depth of 20–25 m, Tégulines Clay is -greenish-grey with rare yellowish aggregates of glauconite that attest to tiny oxidation. Pyrite does not show any sign of oxidation, and carbonates any visible

sign of dissolution. Clay fraction approximatively consists of mixing between kaolinite (39–46 wt%), illite-micas including glauconite (30–34 wt%), chlorite (17–18 wt%) with minor illite-smectite mixed layers (6–10 wt%), and is similar to those defined in well-preserved Tégulines Clay (Fig. 6a, b). Below 20–25 m until 67 m, reduced dark green and compacted Tégulines clay are well preserved. The diagenetic assemblage includes frambooidal pyrite, calcite, glauconite and francolite. Carbonates occur as detrital bioclasts including foraminifers, bivalves and micrite. The largest calcite crystals are present in the carbonate-clay rich unit. The bottom of the clay formation is characterized by the highest clay content (70–72 wt%), 27–29 wt% of quartz – feldspar silty fraction and no carbonate.

6. Cation exchange capacity (CEC)

We measured cation exchange capacity on 68 samples from the seven selected pits where Tégulines Clay was attained at 5 m depth (Fig. 6; supplementary datafile SD2). Samples exhibit a large range of CEC values between 4.4 and 36.9 meq/100 g (Fig. 6a). The highest CEC values up to 37 meq/100 g characterize clay-rich slide surfaces and associated colluvium in the TPH1-1, TV1-4, TV4-3 and TV4-1 pits, and surficial formations overlying carbonate alluvium in the TV1-1 pit. Most clay silty loams have CEC ~ 15–16 meq/100 g. Whitish sandy loam has the lowest CEC values down to 2–4 meq/100 g. At the top of Tégulines Clay, the CEC values are in the range of 18–21 meq/100 g. The lowest values of ~ 12 meq/100 g are measured in Tégulines Clay of the TV4-2 pit. Although CEC values are heterogeneous, the cation distribution in the clay exchange sites is almost homogeneous, with ~ 80 ± 10 % Ca²⁺, ~10–20 % Mg²⁺, and minor K⁺ and Na⁺ (Fig. 6b).

Cation exchange capacity was measured on 54 samples from the four boreholes where Tégulines outcropped or were near surface (AUB260, AUB270, AUB210, AUB230) (Fig. 6c; supplementary datafile SD2). Data from the AUB1010 borehole drilled during the 2015 campaign were added for comparison. The CEC values and cation distribution at exchange sites between 4 and 6 m are very similar to those measured at the top of Tégulines Clay crosscut in pits (Fig. 6c). Below this depth, down to ~ 10–15 m, CEC values slightly decrease to attain homogeneous values of 16 ± 1 meq/100 g through the formation (Fig. 6c). Cation distribution in the clay exchange sites changes with depth, marked by decreasing Ca²⁺ and increasing Mg²⁺, to attain a homogeneous distribution where Ca²⁺ represents ~ 56–58 % of the cations, Mg²⁺ ~31–38 %, K⁺ ~7–9 % and Na⁺ ~1.6–3 %. At the interface with Greensands in boreholes AUB230, AUB210 and AUB1010, CEC values increase, whereas the cation distribution does not change. Comparatively, the average CEC value calculated on 9 samples in Tégulines Clay from the AUB240 borehole that does not outcrop is 19 ± 2 meq/100 g and the cation distribution in the clay exchange sites is almost homogeneous, with ~ 57 ± 1 % Ca²⁺, ~27 ± 1 % Mg²⁺, and minor K⁺ and Na⁺.

7. Waters

Natural reservoirs and groundwaters collected in pits.

Waters were sampled in the reservoirs of “La Carpière” and of “Le Petit Etang” in the paleo-valley of the Brevonne/Aube (Fig. 1b, c). We also sampled 11 groundwaters flowing in pits, when present. Their chemical compositions are given in Table 1.

Groundwaters flowed in all the pits of the first hillslope and in the TV4-1 pit at the bottom of the second hillslope below 3 m. The water flow was important in the TV1-1 and TV1-2 pits, where carbonate alluvium layer was attained. In other pits, the water flow was very small. Groundwaters have pH ranging between 7.4 and 7.9, low ionic strength (Total Dissolved Solids –TDS: <600 mg/L) and are calcic-carbonate waters. Groundwaters of the first slope collected in loam (TV1-3), in

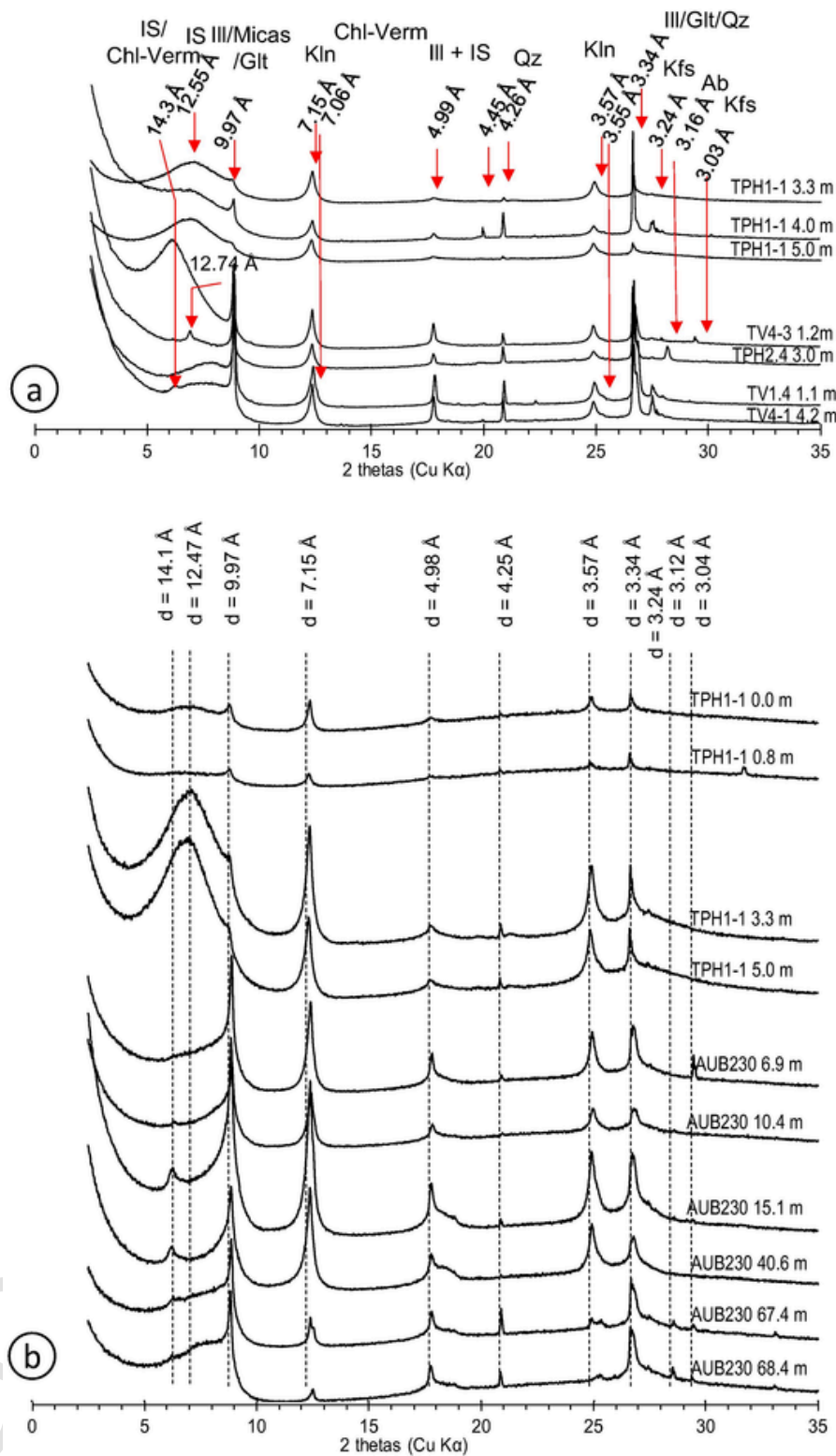


Fig. 5. (a) Normal XRD pattern of the < 2 μm fraction of silty clay loam and top of Tégulines Clay; (b) NEXRD pattern of the < 2 μm fraction of Tégulines Clay at different depths of the AUB230 borehole. Abbreviations: Ab, albite; Chl, chlorite; Ill, illite; IS, illite-smectite mixed layers; Glt, glauconite; Kfs, K-feldspar; Kln, kaolinite; Qz, quartz; Verm, vermiculite.

carbonate alluvium/chalky gravels (TV1-1 at 3 m and TV1-2 at 3 m) and at top of Tégulines in contact with carbonate alluvium/chalky gravels (TV1-1 at 4.8 m and TV1-2 at 4.6 m) have similar chemical compositions and TDS (509–588 mg/L). At the ridge top, groundwaters in the

loam of the TPH1-2 pit and at top of Tégulines Clay of the TPH1-1 pit have pH of 7.4–7.7 and lowest TDS (158–315 mg/L). The TDS at the top of Tégulines Clay of the TPH1-1 pit is slightly higher due to high NO₃⁻ concentration (2 mmol/L).

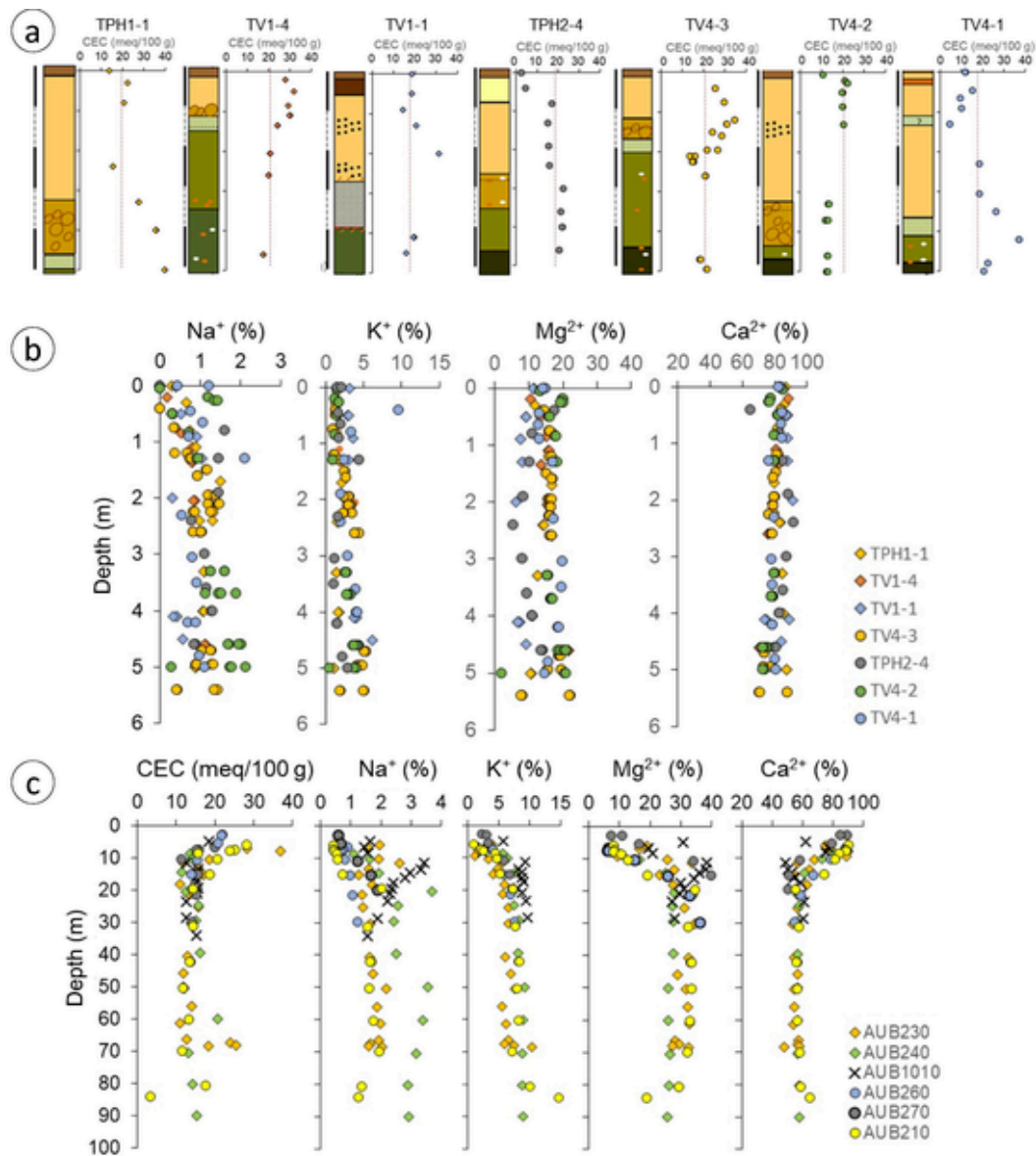


Fig. 6. (a) Profile of cation exchange capacity (CEC) of soils and sediments in function of depth in the seven pits where the top of Tégulines Clay is reached; (b) Distribution of the major cations (Na^+ , K^+ , Ca^{2+} , Mg^{2+}) at exchange sites in soils and sediments of the seven pits where the top of Tégulines Clay is reached; (c) CEC and distribution of the major cations (Na^+ , K^+ , Ca^{2+} , Mg^{2+}) in Tégulines Clay from the five boreholes of the 2018 drilling campaign. The AUB1010 is given for comparison (Lerouge et al., 2018).

Waters of the Carpière reservoir and Le Petit Etang reservoir have low TDS (< 300 mg/L) and are calcic-carbonate waters.

Leaching – chloride, sulfate and nitrate anion concentrations in pore waters of surficial formations and Tégulines Clay crosscut in boreholes.

Anion leaching was realized on 144 samples from the 13 pits and 63 core samples from the five boreholes (AUB210, AUB230, AUB240, AUB260, AUB270). The concentrations of leached anions (Cl^- , SO_4^{2-} and NO_3^-) were measured in leaching of samples with MilliQ water at three solid/water ratios (5, 10 and 20 g/L). They were correlated with solid to liquid ratios, suggesting they were not controlled by mineral dissolution/precipitation and adsorption mechanisms. In that case, the anion concentration in the leachate is linearly proportional with the solid/water ratio, and the linear regression crosscuts zero, and can be used to recalculate anion concentration of pore water in the clay sample as follows: $C_i = \frac{(C_{\text{leached},i} \cdot V/m)}{\omega \cdot \text{anionaccessibility}}$, where i is the anion species (Cl^- , SO_4^{2-} and NO_3^-), $C_{\text{leached},i}$ is the concentration of the i anion in the leachate, V is the volume (in L) of deionized water, m the mass (in g) of

dry powdered clay-rock and ω the water content of the rock at saturation (in $\text{kg}_{\text{water}} \text{kg}_{\text{drysolid}}^{-1}$). The anion accessibility in Tégulines Clay was estimated close to 1 in Lerouge et al. (2018). Anion concentrations in pore waters of all the samples are given in the supplementary datafile SD2. Data from the AUB1010 borehole drilled during the 2015 campaign (Lerouge et al., 2018) were added for comparison.

The Cl^- concentrations in pore waters of soils, loams and Top of Tégulines Clay from 0 to 5 m are generally lower than 5 mmol/L, except in the TPH2-4 pit where values reach 10–15 mmol/L (Fig. 7a). Inferred Cl^- concentrations in pore waters of Tégulines Clay are also low except in the upper part (down to 15 m) of the clay formation in the AUB230 and AUB1010 boreholes (Fig. 7b). The SO_4^{2-} concentrations in pore waters are generally lower than 5 mmol/L in surficial formations, and then slightly increase toward the interface with Tégulines Clay (Fig. 7a). The SO_4^{2-} concentrations are systematically high in the upper part of Tégulines clay formation (down to ~ 15 m); the highest values are measured in the upper part of Tégulines Clay from the AUB230 and

Table 1

Chemical composition of natural groundwaters collected in the pits and in reservoirs (*) of the study area.

	Depth	pH	alkalinity	Na ⁺	K ⁺	Ca ²⁺	Mg ²⁺	Cl ⁻	SO ₄ ²⁻	NO ₃ ⁻
Petit Etang*	m		meq/L	mmol/L	mmol/L	mmol/L	mmol/L	mmol/L	mmol/L	mmol/L
TV4-1	2.4		2.54	0.26		1.04	0.25	0.08	0.15	0.01
TV4-1	3.0		–	0.31	0.02	1.20	0.33	0.09	0.21	
TV4-1	3.3		3.00	0.38		1.31	0.34	0.12	0.31	0.02
Carprière*	0.0		2.57	0.31	0.10	1.31	0.23	0.30	0.29	0.08
TPH1-1	5.4	7.40	1.33	0.57	0.02	1.52	0.21	0.39	0.18	1.99
TPH1-2	3.2	7.54	1.33	0.77		0.58	0.10	0.32	0.14	0.15
TPH1-2	5.0	7.68	1.90	0.87		0.84	0.12	0.39	0.12	0.33
TV1-3	5.2		5.23	0.61		3.08	0.40	0.89	0.40	0.65
TV1-2	3.0	7.90	5.13	0.63		2.82	0.19	0.83	0.36	0.55
TV1-2	4.6		5.44	0.65	0.02	3.00	0.22	0.82	0.38	0.12
TV1-1	3.0	7.47	5.36	0.48	0.37	3.05	0.28	0.60	0.44	0.70
TV1-1	4.8	7.71	4.61	0.54	0.29	2.56	0.30	0.61	0.39	0.57

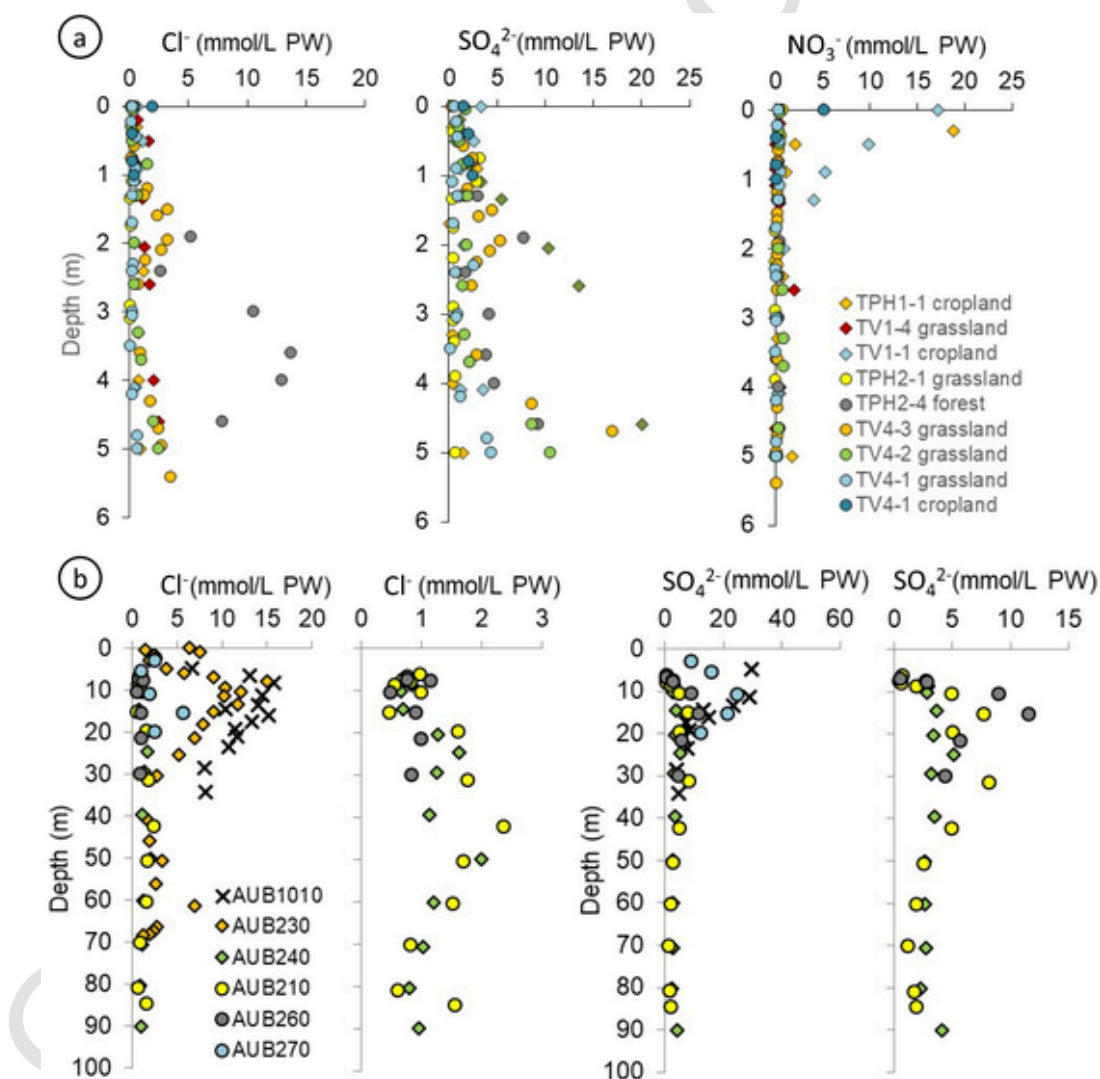


Fig. 7. (a) Concentrations of Cl⁻, SO₄²⁻, NO₃⁻ in pore waters of soils and sediments from the nine 5 m-deep pits; (b) Concentrations of Cl⁻ and SO₄²⁻ in pore waters of Tégulines Clay from the five boreholes of the 2018 drilling campaign. Anion concentrations are given in millimoles of pore waters (mmol/PW). The AUB1010 data (black crosses) are given for comparison (Lerouge et al., 2018).

AUB1010 boreholes (Fig. 7b). Below 15–20 m SO₄²⁻ concentrations decrease to values lower than 5 mmol/L. The NO₃⁻ concentrations in pore waters of surficial formations and top of Tégulines Clay range between 0.01 and 18 mmol/L PW (Fig. 7a). Most of the values in pits dug in grassland are lower than threshold value of 0.80 mmol/L. The highest

values are measured in the first meters of surficial formations in pits dug in cropland (TPH1-1, TV1-1, TV4-1 cropland). The NO₃⁻ concentrations in pore waters of Tégulines Clay are generally lower than 0.03 mmol/L PW.

Dissolved inorganic carbon (DIC) in pore waters.

The sample-degassing protocol was applied to 94 core samples collected in the five boreholes (AUB210, AUB230, AUB240, AUB260, AUB270) and to 54 samples collected in pits. This sampling included only 3 samples of soil, 19 samples of Quaternary loams and 126 samples of Tégulines Clay. The monitoring of the partial pressure of the CO₂ gas (pCO₂) was realized for each sample conditioned in a glass jar until a steady state of the pCO₂ was reached (~2–3 months). The steady state was not reached in soil; the pCO₂ measured at the end of the monitoring was converted in mmole of CO₂ produced per kg of soil. A steady state was reached in Quaternary loams and Tégulines Clay; the pCO₂ measured at the end of the monitoring was converted into a DIC concentration given in mmole of CO₂ per liter of pore water (PW) (supplementary file SD1). An aliquote of each gas was analysed for the carbon isotopic composition of CO₂ ($\delta^{13}\text{C}_{\text{CO}_2}$). All the data are given in the supplementary datafile SD2.

The 3 soil samples are characterized by high CO₂ production of 4.6–10.3 mmole/kg soil and the lowest $\delta^{13}\text{C}_{\text{CO}_2}$ values (~-29 to -25 ‰PDB). The DIC was measured in pore waters of silty clay loam from the TPH1-1, TPH1-2, TPH2-4, TV4-1 and TV4-2. The DIC concentrations range between 0.7 and 6.6 mmol/L PW (Fig. 8a), and the $\delta^{13}\text{C}_{\text{CO}_2}$ values range between -24.6 and -19 ‰PDB (Fig. 8b). The lowest concentrations are measured in the pits at the top of the ridge tops (TPH1-1, TPH1-2, TPH2-4), and the highest ones in the pits at the bottom of the second hillslope (TV4-1 and TV4-2). The DIC concentration measured in pore waters of Tégulines Clay in the five boreholes ranges between 0.3 and 11.6 mmol/L PW. The DIC concentration similarly varies with depth, in all the boreholes (Fig. 8a). The DIC concentration increases rapidly up to 11.6 mmol/L PW from the top of weathered Tégulines Clay down to ~10–12 m and then decreases to become almost constant below 20–25 m (mean value ~1–1.5 mmol/L PW), whatever the borehole. The $\delta^{13}\text{C}_{\text{CO}_2}$ at the top of Tégulines is ~-21 ‰PDB and increases to values up to ~-10 ‰PDB below 20–25 m (Fig. 8).

Pore water chemistry modelling.

We assessed the pore water chemistry in all the Tégulines Clay samples from the pits and AUB240, AUB260 and AUB270 boreholes by equilibration with the mineral assemblage, the DIC and the anion (chloride and sulfate) concentrations and the clay exchanger, according to the THERMOAR Phreeqc model developed by Gaucher et al. (2006; 2009) to model the pore water chemistry of Callovian-Oxfordian Clay, and already applied to Tégulines Clay in Lerouge et al. (2020). The min-

eral assemblage was generally calcite-goethite-gypsum in Tégulines Clay above 10–12 m and calcite-goethite-pyrite below. Pyrite or gypsum were selected based on microscopic observations. Data are given in supplementary datafile SD2.

8. Isotope geochemistry

Oxygen and hydrogen isotopes of pore waters.

A sample of rainfall, surficial waters of the La Carpière and Le Petit Etang reservoirs, and the 11 groundwaters sampled in pits were analysed for oxygen and hydrogen isotopes (supplementary datafile SD2). Rainfall has $\delta^{18}\text{O}$ and δD of -7.6 and -50.8 ‰ vs SMOW. Surficial Waters of the reservoirs show a high ¹⁸O and D enrichment with $\delta^{18}\text{O}$ and δD close to ~0/-1 and -10 ‰ vs SMOW, indicating significant evaporation processes (Fig. 9a, b). The $\delta^{18}\text{O}$ and δD of groundwaters collected in Quaternary loams and Tégulines Clay from 5 m-deep pits of the first hillslope are almost homogeneous, with values ranging between -7.1 and -6.6 ‰ vs SMOW, and between -47.8 and -44.6 ‰ vs SMOW, respectively (Fig. 9a, b). They are slightly isotopically enriched in ¹⁸O and D compared to meteoric waters but are, however, in good agreement with the local and global meteoric water lines (Kloppmann et al., 1998) (Fig. 9c). The $\delta^{18}\text{O}$ and δD of groundwaters collected in Quaternary loams and Tégulines Clay of the TV4-1 pit, at the bottom of the second hillslope, are significantly enriched in ¹⁸O and D compared to meteoric waters, with values ranging between -4.9 and -4.2 ‰ vs SMOW, and between -38.5 and -34.9 ‰ vs SMOW, respectively (Fig. 9c). The $\delta^{18}\text{O}$ and δD of extracted pore waters from Tégulines Clay of the AUB230 borehole ranged between -8.1 and -7 ‰ vs SMOW and between -57 and -50 ‰ vs SMOW, respectively (Fig. 9). They are in good agreement with the local meteoric water line (Fig. 9c). The pore waters $\delta^{18}\text{O}$ and δD at the bottom of the formation are close to Greensands waters (Bougligny) (Innocent et al., 2021) (Fig. 9c).

¹⁴C isotopes of groundwaters.

The ¹⁴C activity was measured in groundwaters of the ancient alluvium in the TV1-1 (4.8 m) and TV1-2 (3 m) pits and in groundwaters at the top of Tégulines Clay on the ridge top of the first hillslope (TPH1-1 – 5.4 m), indicating that they are younger than 50 ky (Table 2). The $\delta^{13}\text{C}$ of DIC of the three groundwaters are almost similar and ~-12 ‰PDB, the value of the natural environment. The ¹⁴C activities correspond to

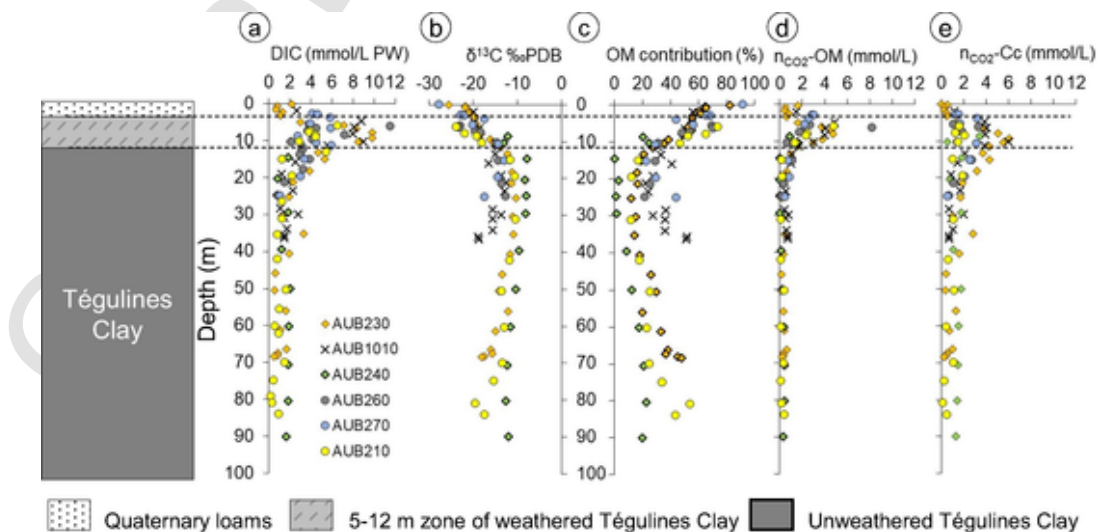


Fig. 8. (a) Profiles of concentration (a) and $\delta^{13}\text{C}$ (b) of inorganic carbon dissolved (DIC) in pore waters of the lithological column including ~5 m of Quaternary formations, weathered Tégulines Clay (~5–12 m zone) and unweathered Tégulines Clay. (c) Profile of organic matter (OM) contribution deduced from the $\delta^{13}\text{C}_{\text{DIC}}$. Profiles of DIC attributed to OM degradation ($n_{\text{CO}_2\text{-OM}}$) (d) and DIC attributed calcite equilibrium ($n_{\text{CO}_2\text{-Cc}}$) (e). Data of the AUB240, AUB230 and AUB1010 boreholes are from Lerouge et al. (2020).

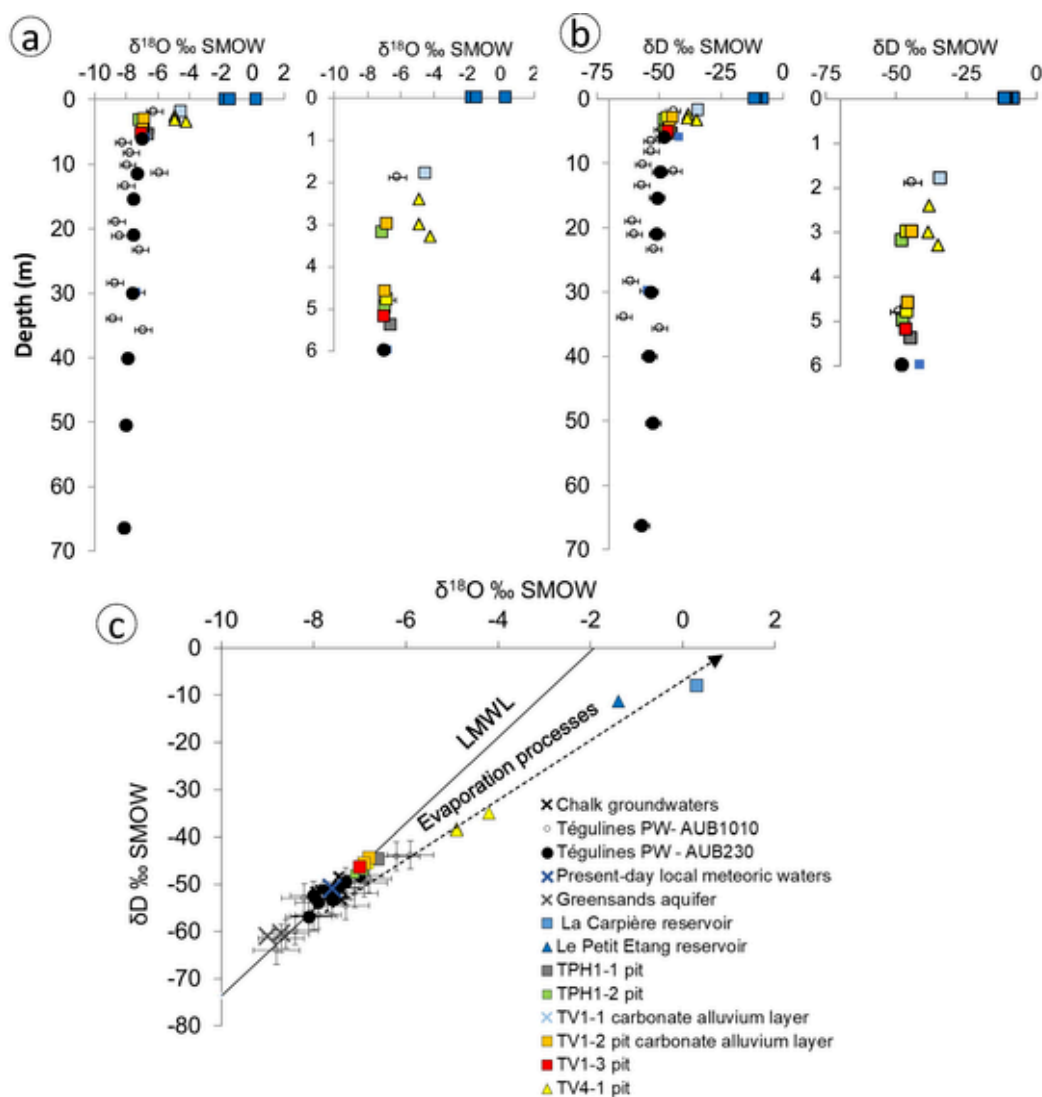


Fig. 9. Groundwaters from pits and pore waters Tégulines from AUB1010 and AUB230 boreholes (a) Profile of $\delta^{18}\text{O}$ with depth; (b) Profile of δD with depth; $\delta^{18}\text{O}$ – δD diagram in which Greensands waters (Innocent et al., 2021), present-day local meteoric waters (water sample provided by Vincent Schneider), chalk waters and the local meteoric water line defined for the Paris Basin Chalk (Kloppmann et al., 1998) are also reported.

Table 2

Carbon data of groundwaters: $\delta^{13}\text{C}$ of dissolved carbonates, ^{14}C activity measured and reported in % of modern carbon normalized taking into account $\delta^{13}\text{C}$ (pCM); carbon, oxygen and strontium data of calcite concretions: $\delta^{13}\text{C}$ and $\delta^{18}\text{O}$ of calcite, $^{87}\text{Sr}/^{86}\text{Sr}$ ratios of calcite, and ^{14}C activity measured and reported in % of modern carbon normalized taking into account $\delta^{13}\text{C}$ (pCM).

	TV1-1 4.8 m	TV1-2 3.0 m	TPH1-1 5.4 m	TPH2-1 1.1 m	TV4-1 4.2 m
Sample type	groundwaters	groundwaters	Groundwaters	concretions	concretions
$\delta^{13}\text{C}$ (‰ PDB) – BRGM				–9.3	–9.6
$\delta^{18}\text{O}$ (‰ SMOW) - BRGM				+26.4	+26.3
$^{87}\text{Sr}/^{86}\text{Sr}$				0.710199	0.707826
$\delta^{13}\text{C}$ (‰ PDB) – dating	–12.3	–11.6	–11.9	–9.1	–7.3
Act ^{14}C pCM	83.8 ± 0.3	64.0 ± 0.2	96.4 ± 0.4	32.82 ± 0.12	1.44 ± 0.04
Conventional age ^{14}C (an BP)	1420 ± 30	3590 ± 30	300 ± 30	8950 ± 30	34060 ± 220
Calendar age				8259–8170 (50 %) 8117–7975 (46 %)	37143–36090 (100 %)

young ages of 1420 ± 30 , 3590 ± 30 and 300 ± 30 years, respectively.

Sr on clay exchanger: concentrations and $^{87}\text{Sr}/^{86}\text{Sr}$.

The concentration and $^{87}\text{Sr}/^{86}\text{Sr}$ ratio of exchangeable strontium were measured in 35 samples in five pits (TPH1-1, TPH2-4, TV1-4, TV1-1, TV4-1), including 4 soils, 19 samples of silty clay loam and 12 sam-

ples of Tégulines Clay at the top of the formation, and 21 core samples from the AUB230 borehole (supplementary datafile SD2). Soils are characterized by the lowest concentrations of exchangeable strontium (0.2–12 ppm) and by the highest $^{87}\text{Sr}/^{86}\text{Sr}$ ratios of 0.7091–0.7105. The exchangeable strontium concentrations range between 2.5 and 42 ppm in silty clay loam, and between 22 and 56 ppm at the top of Tégulines

Clay from pits. The $^{87}\text{Sr}/^{86}\text{Sr}$ ratios of exchangeable strontium range between 0.7085 and 0.7108 in silty clay loam, and between 0.7079 and 0.7084 at the top of Tégulines Clay from pits. In Tégulines Clay from the borehole AUB230, concentrations of exchangeable strontium range between 259 and 1958 ppm and $^{87}\text{Sr}/^{86}\text{Sr}$ ratios between 0.7074 and 0.7081. The profiles of concentration and $^{87}\text{Sr}/^{86}\text{Sr}$ ratio of exchangeable strontium in function of depth shows a decrease of the concentrations and an increase of $^{87}\text{Sr}/^{86}\text{Sr}$ ratio from the top of Tégulines Clay toward the surface (Fig. 10a, b).

Calcite concretions.

Two concretions of calcite sampled in pits TPH2-1 at 1.1 m and TV4-1 at 4.2 m were analysed for their $\delta^{13}\text{C}$, $\delta^{18}\text{O}$, $^{87}\text{Sr}/^{86}\text{Sr}$ and ^{14}C (Table 2). The $\delta^{13}\text{C}$ and $\delta^{18}\text{O}$ of both concretions are very similar, ~ -9 ‰ PDB and $\sim +26$ ‰ vs SMOW. Conversely, their $^{87}\text{Sr}/^{86}\text{Sr}$ ratios are different: 0.71020 for TPH2-1 1.1 m and 0.70783 for TV4-1 4.2 m.

The ^{14}C activity was measured in both concretions, confirming that they are younger than 50 ky. The $\delta^{13}\text{C}$ of calcite aliquot used for the age measurement of the concretion TPH2-1 at 1.1 m is in good agreement with the value we measured in our laboratory. Its ^{14}C activity corresponds to a young age of 8 ky for the concretion TPH2-1 at 1.1 m. The $\delta^{13}\text{C}$ of calcite aliquot used for the age measurement of the concretion TV4-1 at 4.2 m is slightly higher than the value we measured at the laboratory, indicating it probably contains a contribution of ancient marine carbonate. Consequently, the age of this concretion is probably younger than the age of ~ 37 ky estimated from the ^{14}C activity.

9. Discussion

9.1. Pore water chemistry in the critical zone

Major ion chemistry of surficial waters and ground water combined with local geology has been widely used to study subsurface hydrogeochemical processes (Cherchali et al., 2022; Cloutier et al., 2008; Gao et al., 2019; Kumar and James, 2016; Lakshmanan et al., 2003; Li et al., 2013; Sun et al., 2021). Hereafter surficial waters, ground waters and pore waters of surficial formations and Tégulines Clay of this study, as well as available data of pore waters obtained by squeezing of Tégulines Clay (Lerouge et al., 2018, 2020), were used to constrain hydrogeochemical processes and water/sediment interactions at the scale of the area.

Waters of the reservoirs in the paleo-valley and groundwaters collected in pits of the first hillslope and at the bottom of the second hillslope have low ionic strength (Total Dissolved Solids –TDS: < 600 mg/L) and are calcic-carbonate waters according to the Piper's classification (Fig. 11a). Their low Mg/Ca ratios, significantly lower than 1, their relative high alkalinity and $\delta^{13}\text{C}$ (~ -12 ‰ PDB) are characteristic of sub-oxic groundwaters (Bohlke and Horan, 2000). Water chemical composition of the Carpière reservoir is almost similar to that of groundwaters of the first ridgetop (TPH1-1 and TPH1-2), while water chemical composition of Le Petit Etang reservoir is almost similar to that of the groundwaters of the TV4-1 pit in the paleovalley.

Tégulines Clay pore waters (squeezing and calculated) have chemical compositions and TDS different from those of groundwaters. They are dominantly Ca-Mg-SO₄-rich according to the piper's classification (Fig. 11b), and have significantly higher TDS than groundwaters and loam pore waters. We reported Tégulines Clay pore waters in a Gibbs diagram to illustrate their high variability of TDS (592–6457 mg/L) and

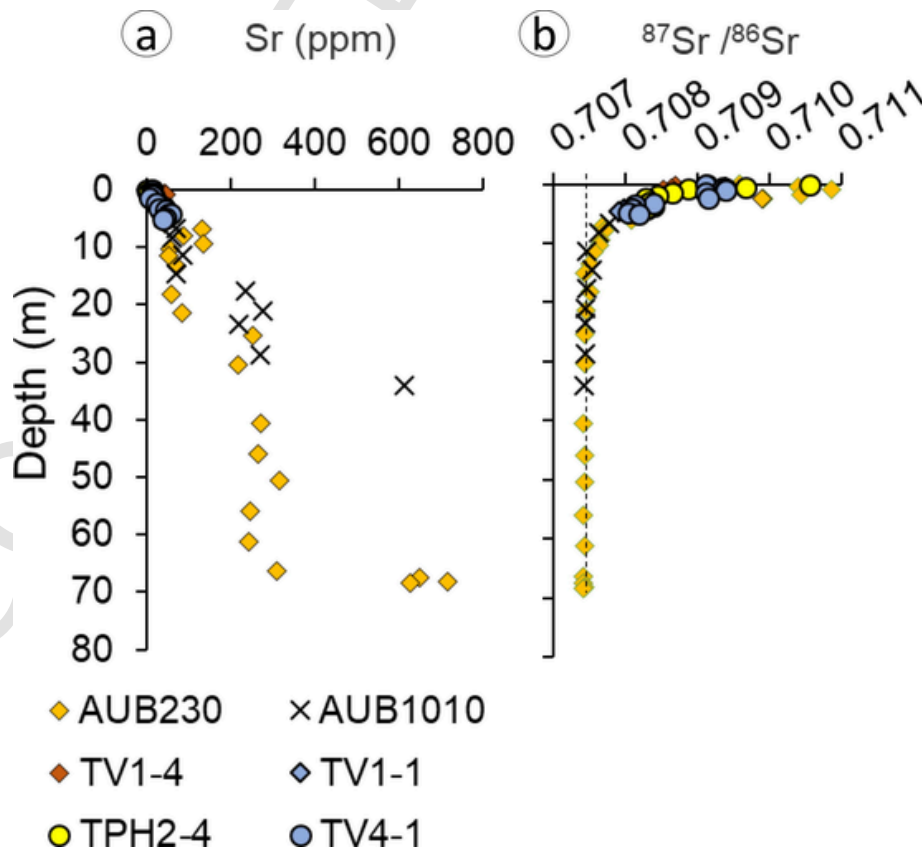


Fig. 10. (a) Profile of concentrations of exchangeable strontium of sediments from 5 pits and the AUB230 borehole; (b) Profile of $^{87}\text{Sr}/^{86}\text{Sr}$ ratio of exchangeable strontium of sediments from 5 pits and the AUB230 borehole. Data of the Tégulines Clay from the AUB1010 borehole are given for reference (Lerouge et al., 2018).

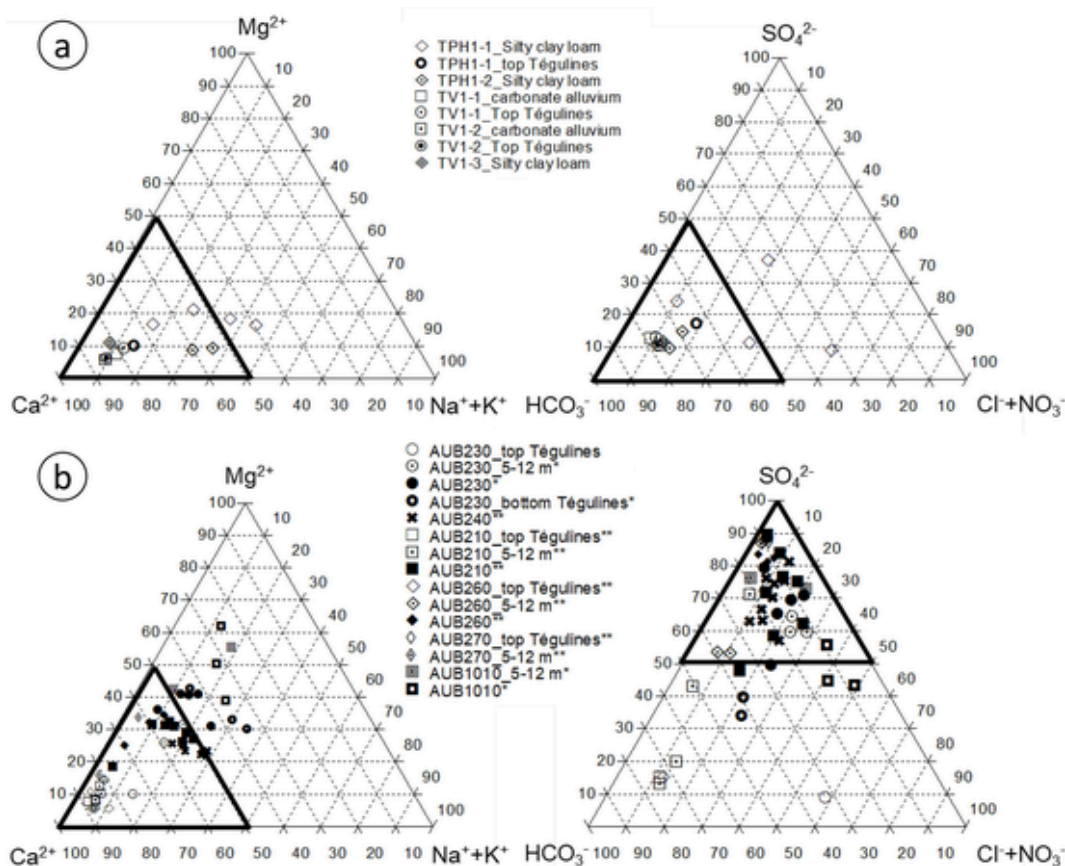


Fig. 11. Ca^{2+} - Mg^{2+} - $(Na^{+}+K^{+})$ and HCO_3^{-} - SO_4^{2-} - $(Cl^{-}+NO_3^{-})$ ternary diagrams showing the chemical composition of (a) surficial waters, groundwaters and pore waters at top of Tégulines Clay, and (b) Tégulines Clay porewaters from the different boreholes (AUB230, AUB1010, AUB210, AUB260, AUB270).

to relate them for determining major processes controlling their chemistry (Fig. 12a). Pore waters of unweathered clay crosscut in the AUB240 borehole have the lowest TDS (627 ± 100 mg/L), associated with the lowest Cl^{-} concentrations (1.3 mmol/L), DIC concentrations (1.5 mmol/L) and SO_4^{2-} concentrations (6.5 mmol/L). Pore waters in the lower part of Tégulines Clay in the boreholes AUB210 and AUB260 are quite similar to that of the AUB240 reference, and plot in the domain of water–rock interactions of the Gibbs diagram for cations and anions (Fig. 12a). Pore waters of the weathered Tégulines Clay in the ~ 5–12 m zone (including the top of the formation) of all the boreholes exhibit larger chemical variations than unweathered clay; they have the highest TDS (2263–6457 mg/L) associated with the highest Cl^{-} concentrations (up to 22 mmol/L), DIC concentrations (up to 11.6 mmol/L), and SO_4^{2-} concentrations (up to 77 mmol/L). Most of these pore waters also plot in the field of water–rock interactions, excepted pore waters of the AUB1010 and AUB230 that plot in the field of evaporation processes for anions and out of the field for cations. At the top of the Tégulines Clay in contact with loams, chemistry of clay pore waters tends to be richer in Ca^{2+} and in DIC, and is closer to that of loams.

The weathering intensity and the depth of the weathering profile vary a lot along the two successive hillslopes separated by a small valley that is the paleo-valley of the Aube/La Brevonne River (Fig. 13). According to the TDS spatial distribution, the most intense weathering processes seem to have developed under the first ridge top and the low east-facing slope of the Aube/Brevonne paleo-valley. On the ridgetop of the second west-facing hillslope (AUB210, AUB260 boreholes), the weathering intensity is lower, and pore waters are a little modified. The increase of the ionic strength is associated with the combined increase of the Cl^{-} , DIC and SO_4^{2-} concentrations. The increase of the Cl^{-} concentrations is important in the paleo-valley between the AUB230 and

AUB1010 boreholes, while the DIC and SO_4^{2-} concentrations increase more homogeneously in the upper part of Tégulines Clay down to ~ 12 m, and independently of the position in the slopes.

Here data provide evidence of a significant increase of Cl^{-} concentrations in Tégulines Clay pore waters in the 5–12 m zone of AUB1010 borehole, AUB230 borehole and TPH2-4 pit and to a lesser extent in Quaternary loam (TPH1-1) pore waters overlying Tégulines clay of the AUB230 borehole. The Cl^{-} enrichment affects Tégulines Clay to a less extent below 12 m down to ~ 20–30 m in the two boreholes and consequently affects quite all the thickness of the clay in the AUB1010 borehole. Because TPH1-1 pit, and AUB230 and AUB1010 boreholes were drilled in cropland, a contribution of anthropogenic Cl^{-} coming from fertilizers cannot be ruled out. However, based on the transport parameters (porosity and permeability) of surficial formations and Tégulines Clay (ANDRA, 2015), diffusion from the surface seems unlikely to explain such high concentrations of chloride down to 20–30 m in the two boreholes.

The enrichment in Cl^{-} of pore waters is correlated with high DIC and SO_4^{2-} measured in AUB230 and AUB1010 boreholes. This general enrichment inducing high TDS could be attributed to an evaporation process as shown previously in the Gibbs diagram for anions but not for cations. Evaporation results in an increase of TDS concentrations at constant Na^{+}/Cl^{-} ratios. In our case, most of the Cl^{-} -rich pore waters in AUB230 and AUB1010 boreholes show an increase of TDS concentrations, but have a Na^{+}/Cl^{-} ratio significantly lower than 1 (Fig. 12b), giving evidence of other processes than evaporation. Evaporation processes strongly suggest an ancient period of warm and dry climate. These conditions favour the occurrence of ionic exchange during the recharge of Ca^{2+} -rich groundwaters in presence of clay minerals with high cation exchange capacities (CEC), and Na^{+} on their exchange sites (Cloutier et al., 2010). The negative correlation between Na^{+}/Cl^{-} and

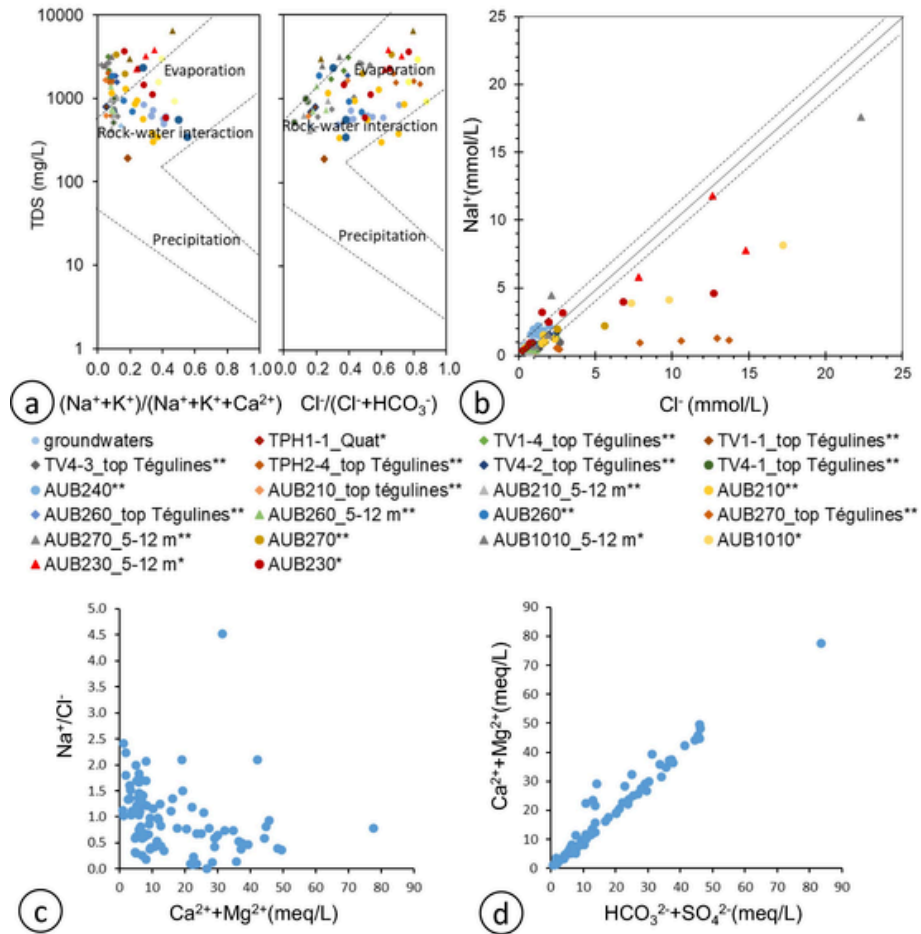


Fig. 12. (a) Gibbs plot highlighting the geochemical processes in groundwaters and Tégulines Clay pore waters; (b) Na⁺-Cl⁻ diagram in which groundwaters and Tégulines pore waters are reported; (c) Na⁺/Cl⁻ ratio in function of Ca²⁺+Mg²⁺ diagram in which Tégulines pore waters are reported; (d) Ca²⁺+Mg²⁺ in the function of HCO₃⁻+SO₄²⁻ diagram in which Tégulines pore waters are reported.

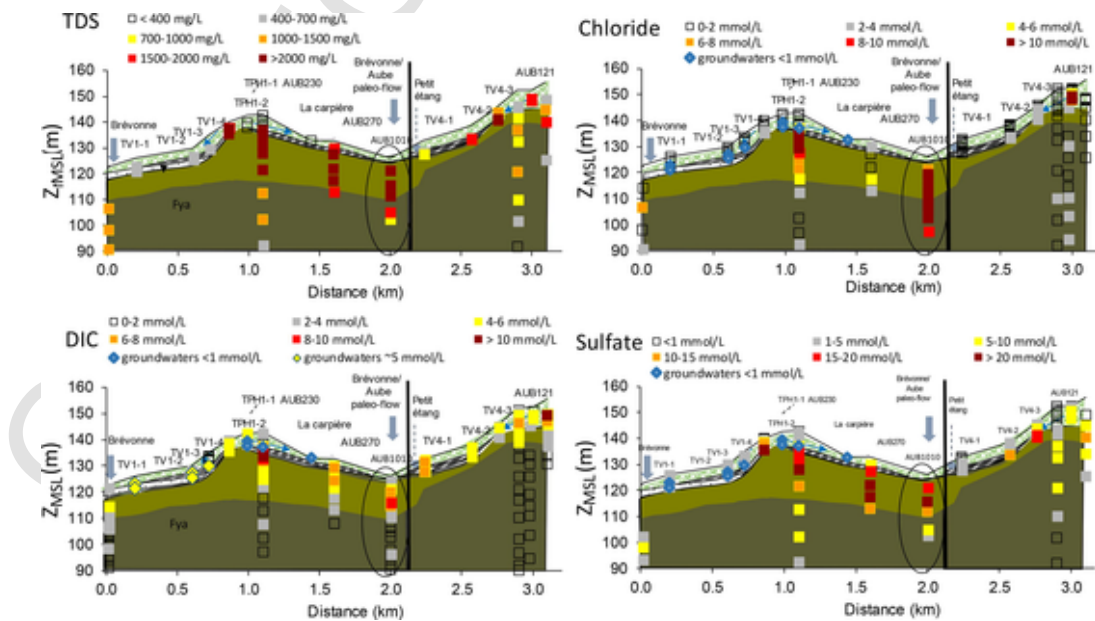
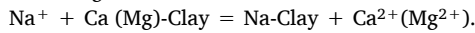


Fig. 13. Distribution of TDS and concentrations of Cl⁻, DIC and SO₄²⁻ along the two successive hillslopes and with depth.

$\text{Ca}^{2+} + \text{Mg}^{2+}$ highlights ion exchange processes (Fig. 12c). Two types of ion exchange, normal and reverse, are identified by reporting pore waters in a $\text{Ca}^{2+} + \text{Mg}^{2+}$ vs $\text{HCO}_3^- + \text{SO}_4^{2-}$ diagram with a 1:1 mixing line (Rajmohan and Elango, 2004). In our case, pore waters are on or above the mixing line, towards the $\text{Ca}^{2+} + \text{Mg}^{2+}$ field, indicating that reverse ionic exchange processes are dominant (Fig. 12d), according to the following reaction:



The enrichment in sulfates in pore waters of Tégulines Clay in the weathered zone down to ~ 12 m is consistent with the observation of gypsum and iron hydroxides (ferrihydrite, goethite) in replacement of early pyrite (Lerouge et al., 2018). The formation of such phases with higher molar volume (ferrihydrite $34.36 \text{ cm}^3\text{-mol}^{-1}$; Blanc et al. 2012; goethite $20.82 \text{ cm}^3\text{-mol}^{-1}$; gypsum) than pyrite ($23.94 \text{ cm}^3\text{-mol}^{-1}$), and containing variable amounts of water induces: 1) a volume expansion that can contribute to the increase of porosity (Gu et al., 2020), but also: 2) a higher sensitivity to hydrometric conditions that can significantly modify mechanical properties such as plasticity (Lerouge et al., 2018). The increase of porosity and changes in mechanical properties induced by the oxidation of pyrite are two major factors influencing water and gas diffusion rates through the critical zone.

10. Natural isotopic tracers

Oxygen and hydrogen isotopes of waters.

The Tégulines Clay pore waters below ~ 6 m lie next to the LMWL and GMWL (Local and Global Meteoric Water Lines) (Kloppmann et al., 1998), indicating that meteoric waters have diffused through the clay formation during post-depositional history and replaced original connate seawater (Fig. 9b). The $\delta^{18}\text{O}$ and δD of pore waters of Tégulines Clay below 6 m are almost similar to present-day local meteoric waters. The $\delta^{18}\text{O}$ and δD of pore waters at the bottom of the clay formation are similar to those of the Greensands aquifer. Above ~ 5–6 m, the $\delta^{18}\text{O}$ and δD of groundwaters and Tégulines Clay pore waters in the 5 m-deep pits of the first hillslope and in the TV4-1 pit at the bottom of the second hillslope show an ^{18}O and D enrichment. Groundwaters of the first hillslope are near the LMWL, while groundwaters of the TV4-1 pit plot along a line with a slope of 5.87 between rainfall on the LMWL and the reservoirs of La Carpière and Le Petit Etang, indicating that groundwaters and reservoirs are affected by evaporation processes. Groundwaters of the first hillslope are slightly enriched in ^{18}O and D, probably due to regular recharge by meteoric waters.

Strontium isotopes of exchangeable strontium.

Strontium isotopes, when coupled with Sr concentrations, are a good monitor of geochemical processes in natural clayey formations (Lerouge et al., 2010), and are also used to investigate the mixing of different groundwaters (Négre et al., 2001; Sullivan et al., 2016; Demonterova et al., 2022). The $^{87}\text{Sr}/^{86}\text{Sr}$ of exchangeable strontium is representative of strontium in present-day pore waters of clay-rich formations (Lerouge et al., 2010). In unweathered and slightly weathered Tégulines Clay from boreholes AUB1010 and AUB230 below 12 m, $^{87}\text{Sr}/^{86}\text{Sr}$ ratio of exchangeable strontium ranges between 0.7074 and 0.7075, with a mean value of 0.707438 ± 0.000034 . This range of values is consistent with the Lower Cretaceous seawater (Jones and Jenkyns, 2001), suggesting a limited diffusion of Sr since the formation deposition. In weathered Tégulines Clay, $^{87}\text{Sr}/^{86}\text{Sr}$ ratio of exchangeable strontium slightly increases from 0.7075 to 0.7084 at the top of the formation. The $^{87}\text{Sr}/^{86}\text{Sr}$ ratios of exchangeable strontium of overlying silty clay loam are 0.7085–0.7109. The decreasing of strontium content on the exchangeable fraction at the top of Tégulines Clay coupled with the increasing $^{87}\text{Sr}/^{86}\text{Sr}$ ratio suggests a slight dilution of Téguline Clay pore waters by groundwaters of overlying silty clay loam.

DIC, $\delta^{13}\text{C}$ of DIC and carbonates and ^{14}C activity.

The chemical contrast between groundwaters and pore waters in silty clay loam, which are diluted waters, and Tégulines pore waters in-

dicate that DIC concentrations at the top of the Tégulines Clay down to ~ 10–12 m are not due to diffusion of surficial pore waters into the clays.

The DIC increases rapidly up to 10 mmol/L from the top of weathered Tégulines Clay down to ~ 10–12 m and then decreases to become almost constant below 20 m (~1–1.5 mmol/L PW), whatever the borehole. The $\delta^{13}\text{C}_{\text{CO}_2}$ at the top of Tégulines is ~ -21 ‰ PDB and increases to values of ~ -10 ‰ PDB at 15–20 m (Fig. 8). The highest values are consistent with $\delta^{13}\text{C}_{\text{CO}_2}$ calculated at equilibrium with calcite ($\delta^{13}\text{C}_{\text{CO}_2\text{-calcite}} \sim -10 \text{ ‰ PDB}$) (Lerouge et al., 2020). The large $\delta^{13}\text{C}_{\text{CO}_2}$ range (-19.8 to -10.5 ‰) of the weathered Tégulines Clay indicates a mixed origin of CO_2 component internally controlled by the equilibrium between pore waters and calcite ($\delta^{13}\text{C}_{\text{CO}_2\text{-calcite}} \sim -10 \text{ ‰ PDB}$), and CO_2 release by the degradation of organic matter ($\delta^{13}\text{C}_{\text{CO}_2\text{-organic matter}} \sim -29 \text{ ‰ PDB}$). We estimate the contributions (in %) of the organic matter degradation ($X_{\text{organic matter}}$) and CO_2 due to calcite equilibrium (X_{calcite}) to DIC, and the corresponding concentrations $n_{\text{CO}_2\text{-OM}}$ and $n_{\text{CO}_2\text{-C}}$ given in mmol/L for each $\delta^{13}\text{C}_{\text{CO}_2}$ of clay sample (Fig. 8). The data give evidence of a CO_2 peak due to organic matter at the top of the clay and a CO_2 peak due to calcite equilibrium in the 5–12 m zone. This latter is significantly higher than DIC in unweathered Tégulines Clay, in agreement with the dissolution of marine carbonates, and more specifically carbonate bioclasts, in highly reactive Tégulines Clay (Lerouge et al., 2018).

It is noteworthy that in most of the pits where the loam/clay boundary is accessible, secondary carbonates rapidly precipitated as a fine calcite layer close to the boundary when the contact is stable, and as concretions in Tégulines Clay when a slide plan separates clay from the surficial formation. Rare secondary carbonates also precipitated in cracks affecting loam at the ridgetop of the secondary hillslope (TPH2-1/AUB210). The position of the secondary carbonates probably informs on the water table limit. The morphology of calcite precipitates rather depends on the sedimentary rock texture. A fine layer of calcite homogeneously precipitated in microporosity of top of the Tégulines clay when rock microstructures were modified a few, and rock was weathered a few. Concretions and precipitations in cracks precipitated in sedimentary rocks when rock texture was highly modified by weathering and dessication in unsaturated zone.

The $\delta^{13}\text{C}$ and $\delta^{18}\text{O}$ of the concretions at the top (TPH2-1) and the bottom (TV4-1) of the second hillslope allowed calculating $\delta^{13}\text{C}$ and $\delta^{18}\text{O}$ of fluid from which they precipitated, using the carbon and oxygen isotopic fractionations between calcite and water at 20 °C, respectively 2 ‰ (Deines et al., 1974) and 29.1 ‰ (Kim and O'Neil, 1997). The $\delta^{13}\text{C}_{\text{fluid}}$ value of -11.5 ‰ PDB, the $\delta^{18}\text{O}_{\text{fluid}}$ value of -3 ‰ vs SMOW and $^{87}\text{Sr}/^{86}\text{Sr}$ ratios of the concretions show that secondary calcite concretions are isotopically at equilibrium with groundwaters that were affected by an intense evaporating process. The ^{14}C activity of both concretions confirms their old ages, the oldest one at ~ 34 ky in the TPH2-1 pit at the ridgetop of the second hillslope and a younger age of ~ 8 ky in the TV4-1 pit at the bottom of the hillslope. Even though high DIC are well correlated in-depth with quite a recent mineral reactivity and organic matter (OM) degradation, previous DIC profile chemical modelling using Phreeqc program needed to take into account evaporation processes in association with mineral and OM reactivity to explain the high DIC values measured in AUB230 and AUB1010 boreholes (Lerouge et al., 2020).

11. Nitrates as tracer of anthropic activity

Natural nitrate concentrations in surficial and groundwaters are estimated to 5 to 15 mg/L (0.08–0.24 mmol/L; Brenot et al., 2008). The use of nitrogen fertilizers has significantly increased the diffuse nitrate loading of surface waters and groundwaters in agricultural areas. The regulatory limit for nitrate in drinking water is 10 mg/L as nitrate-nitrogen ($\text{NO}_3\text{-N}_2$), and is approximately equivalent to the World

Health Organization (WHO) guideline of 50 mg/L (0.8 mmol/L) as NO_3 (Ward et al., 2018).

Nitrate concentrations in all the Tégulines Clay pore waters from boreholes are low and in the range of natural waters. Nitrate concentrations in loams overlying Tégulines Clay vary from site to site. Significant high values (up to 18 mmol/L PW) are measured by leaching of soil samples of pits TPH1-1, TV1-1 and TV4-1 dug in cropland in October 2017, while in other pits dug in grassland, values rarely exceed the regulatory limit for nitrate in drinking water (supplementary figure SD3). Nitrate concentrations rapidly decrease below the regulatory limit at ~ 1–1.3 m in the three pits dug in cropland. The decrease is faster in the TPH1-1 and TV4-1 than in the TV1-1 pit which is the present-day Brevonne-Aube valley. The 1–1.3 m depth corresponds to the depth of the drainage system that was installed in the 1980's and probably helps nitrates to migrate to the discharge zone.

It is noteworthy that concentrations measured in waters extracted by squeezing of core samples in December 2017 are lower than that obtained by leaching of equivalent samples dug in the TPH1-1 pit in October 2017, probably suggesting the contribution of a soluble nitrate form during leaching. Nitrate can act as an oxidant only if microorganisms are present (Bosh et al., 2012) in the system that is likely at a shallow depth where it reaches a maximum of 1.70 m and is barely detectable below 2.40 m. Then, oxygen is the more abundant oxidant and reaches its maximum at 5 m and is still present at 10 m (Lerouge et al., 2020). The weathering is thus rate-limited by oxygen, especially at the hilltop and to a lesser extent in the valley where the nitrate concentration can be much more important (~17 mmol/L at 5 m in AUB1010 but not present anymore at 10 m).

12. Weathering profile and hydrology in the studied area

The studied area is very close and upstream of the hydrological chalk watershed extending from the reservoir's dams to Pont-sur-Seine of the Seine-Aube confluence (Fig. 14a) (Bendjoudi et al., 2002). Combining fieldwork with petrological and geochemical data allows a better understanding the current hydrological system functioning at the scale of the studied area. The variations of present-day topography and slope angle influence the water flow direction, and flow accumulation, and allow defining of the recharge and discharge zones. The present-day topography and the hydrographic network result from the successive river banks developed later than the Oligocene-Eocene erosion surface and associated with major climatic cycles during Quaternary. The age of the lowest fluvial terrace (Fya) above the Aube major bed on the east of the studied area is ~ 300–165 ky (Voinchet et al., 2015).

The pit-digging campaign in October 2017 provided evidence of groundwaters in ~ 5 m –deep pits between the bottom of the second hillslope and the bottom of the first hillslope near the Brevonne River. The ^{14}C ages of three groundwaters (TPH1-1, TV1-1, TV1-2) are lower than 10 kyrs, and consequently younger than the last ice age. The shallow groundwaters at the first ridgetop (TPH1-1 5.4 m) correspond to a temporary perched water table that is favoured by the increase of the clay content and particularly of smectite in the succession of Quaternary clay loams and colluvium overlying Tégulines Clay, as observed in the TPH1-1 pit/AUB230 borehole (Fig. 14b). Their youngest age of 300 years indicates that the ridgetop constitutes a current zone of recharge. Rainfalls falling on this relief infiltrate Quaternary loams and laterally flow for one part along the first west-facing hillslope of the present-day Brevonne valley, and another part along the east-facing hillslope of the Brévonne/Aube paleo-valley (Teles et al., 2004; Voinchet et al., 2015). The steeper west-facing slope promotes landslide by gravity (TV1-1, TV1-2), drainage and runoff of waters towards the Brevonne Valley, which is a discharge zone belonging to the present-day Aube alluvium plain and at a larger scale to the Seine-Aube confluence (Fig. 14a). The groundwaters of the TV1-2 and TV1-1 pits were collected in carbonate alluvium, corresponding probably to the ancient

Aube Fya fluvial terrace observed at the east (165–300 kyrs; Voinchet et al., 2015). Their $\delta^{13}\text{C}$, $\delta^{18}\text{O}$ and δD are similar to that of groundwaters of the ridgetop, suggesting that all the waters have the same origin, have evolved in the same environment and are isotopically equilibrated with the carbon system. The groundwater $\delta^{18}\text{O}$ and δD are slightly enriched compared to meteoric waters, corresponding to ~ 5–10 % of evaporation. However, they are chemically different and older. Groundwaters of the recharge zone are more diluted and less calcic than that of the slope and that of the discharge zone, strongly suggesting water/sediment interactions toward the discharge zone. In that case, we cannot neglect the possibility of contamination of ancient carbon source (^{14}C -free) increasing ^{14}C age.

The almost flat morphology of the east-facing slope and the bottom of the west-facing slope of the Brevonne/Aube paleo-valley is more likely to collect stagnant waters that can invade the loamy horizon of the paleo-valley during wet periods. The presence of small reservoirs such as the “La Carpière” and of “Le Petit Etang” reservoirs and the installation of drainage in the cropland on the east-facing slope is consistent with wetlands. The paleo-valley has an altitude slightly higher than the current Aube/Brevonne Valley and is connected to the Voire Valley at the north and the Brevonne Valley at the south. It does not belong to the current Aube alluvium plain. However, its position at the confluence of the two rivers is included in the Aube widespread floodplain invaded during exceptional raining events, as attest by the deposits of quaternary loams on the ridgetops, as well as silty loams of the studied area. The $\delta^{18}\text{O}$ and δD of reservoirs (natural or created for drainage) with values evolving to seawater signature during the dry period (summer) are significantly enriched compared to meteoric waters, indicating important evaporation processes. The groundwater $\delta^{18}\text{O}$ and δD collected in the paleo-valley are probably a mixing between these evaporated waters, waters of the recharge zones and runoff waters during wet seasons (autumn to spring). All these data rather suggest that the paleo-valleys of the area represent large intermediate discharge zones between the coarse ridgetops (recharge zones) and the current Aube alluvium plain.

13. Conclusions

A field campaign including twelve 5 m-deep pits and five deep (30–90 m) boreholes was conducted in the area of Brienne-Le-chateau, at the east of the Aube alluvium plain (France). The pit-digging campaign along two-stepped west-facing hillslopes along the Brevonne valley and the Aube/Brevonne paleo-valley showed that thin Quaternary clay silty and carbonate-free loams cover Tégulines Clay in all the area. Their thickness varies between ~ 1–2 m on the upper part of the hillslopes to 5–10 m on the top of the two east-facing hillslopes. Landslides of clay loams and Tégulines Clay displaced downslope. One meter-thick layer of chalky gravel covers Tégulines Clay in the valley of the Brevonne River. The pit digging also allowed collecting groundwaters in ~ 5 m –deep pits between the bottom of the second hillslope and the bottom of the first hillslope near the Brevonne River. Groundwaters have low TDS concentrations (< 600 mg/L), and are calcic-carbonate water-type. The distribution of groundwaters and their ^{14}C ages provided evidence of a current zone of recharge and temporary perched water table at the first ridgetop, and recent lateral groundwater transfers and runoff of waters along the first west-facing steep slope toward the Brevonne River, which is a discharge zone belonging to the present-day Aube alluvium plain. The perched water table is favoured by the increase of the clay and smectite contents in the Quaternary clay loams and colluvium overlying Tégulines Clay. Groundwaters of the recharge zone are more diluted and less calcic than that of the slope and that of the discharge zone, strongly suggesting water/sediment interactions toward the discharge zone.

Combined petrological and geochemical studies of Tégulines Clay from deep boreholes showed that the weathering intensity and the

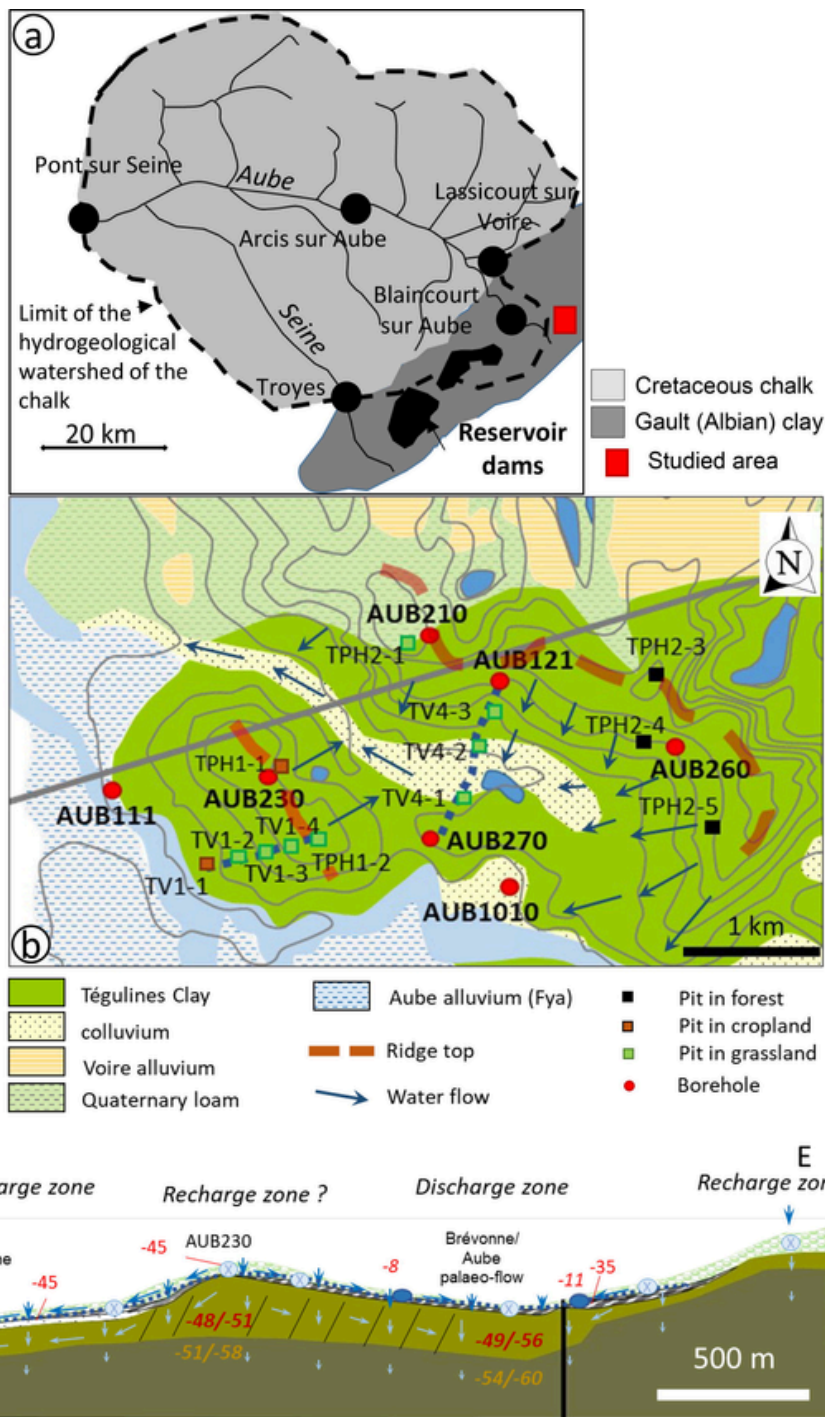


Fig. 14. (a) Location of studied area and the hydrogeological watershed of the Chalk; (b) Geological and topologic map in which water flows are indicated. (d) E—W profile through the CZ developed in Tégulines Clay in which direction of water flow are reported by blue arrows. The dashed zone corresponds to the zone of weathered Tégulines Clay. δD of waters are written in red/orange italic. (For interpretation of the references to colour in this figure legend, the reader is referred to the web version of this article.)

depth of the weathering profile vary a lot along the two successive hillslopes highlighting the need to acquire data at the watershed scale to be able to understand its 3D-functioning. The pore water chemistry of Tégulines Clay differs from that of groundwaters. They are Ca^{2+} - Mg^{2+} - SO_4^{2-} -rich water-type and show a large range of TDS concentrations (592–6457 mg/L). The highest values are measured in the most intensely weathered clays that developed in the first 10–15 m under the first ridge top and the low east-facing slope of the Aube/Brevonne paleo-valley. On the ridgetop of the second west-facing hillslope, the

weathering intensity is low, and pore waters are little modified. The Aube/Brevonne paleo-valley could represent a large intermediate discharge zone between the coarse ridgetops (recharge zones) and the current Aube alluvium plain, included in the Aube widespread floodplain and invaded during exceptional raining events. The high ionic strengths combined with high $\delta^{18}O$ and δD water values measured in Tegulines clay pore waters of this paleo-valley suggest ancient important evaporation processes associated with a cation exchange from the clay exchange sites. Finally, the data obtained in the present study enable us to

understand the flow paths of the studied watershed, which is closely linked to the mineralogical transformation. This helped to get a comprehensive description of the major processes that will govern that watershed functioning.

Uncited references

Abdalla (2009), Arizaleta et al. (2020), Böhlke and Horan (2000), Bosch et al. (2012), Bromley et al. (1997), Fernández et al. (2014), Jankowski and Acworth (1997), Milesi et al. (2020), Sajil Kumar and James (2016), Sebilo et al. (2013), Subramani et al. (2010), Voinchet et al. (2012).

Declaration of Competing Interest

The authors declare that they have no known competing financial interests or personal relationships that could have appeared to influence the work reported in this paper.

Data availability

Data will be made available on request.

Acknowledgements

The French National Radioactive Waste Management Agency (ANDRA) and the French Geological Survey (BRGM) supported this study through the GAULT_ZC 2017-2018 project n°20073040. We thank Editor in chief, Dr Sally Thompson, and three anonymous referees for their constructive comments and significant improvements to the manuscript.

Appendix A. Supplementary data

Supplementary data to this article can be found online at <https://doi.org/10.1016/j.jhydrol.2023.129077>.

References

- Abdalla, O.A.E., 2009. Groundwater recharge/discharge in semi-arid regions interpreted from isotope and chloride concentrations in north White Nile Rift. Sudan. *Hydrogeol. J.* 17, 679–692.
- Arizaleta, M.L., Nightingale, M., Tutolo, B.M., 2020. A rate law for sepiolite growth at ambient temperatures and its implications for early lacustrine diagenesis. *Geochim. Cosmochim. Acta* 288, 301–315.
- Bao, Z., Haberer, C.M., Maier, U., Amos, R.T., Blowes, D.W., Grathwohl, P., 2017. Modeling controls on the chemical weathering of marine mudrocks from the Middle Jurassic in Southern Germany. *Chem. Geol.* 459, 1–12.
- Bendjoudi, H., Weng, P., Guérin, R., Pastre, J.F., 2002. Riparian wetlands of the middle reach of the Seine river (France): historical development, investigation and present hydrologic functioning. A case study. *J. Hydrol.* 263, 131–155.
- Böhlke, J.K., Horan, M., 2000. Strontium isotope geochemistry of groundwaters and streams affected by agriculture, Locust Grove, MD. *App. Geochem.* 15, 599–609.
- Bolton, E.W., Berner, R.A., Petsch, S.T., 2006. The Weathering of Sedimentary Organic Matter as a Control on Atmospheric O₂: II. Theoretical Modeling. *American J. Sci.* 306, 575–615.
- Bosch, J., Lee, K.Y., Jordan, G., Kim, K.W., Meckenstock, R.U., 2012. Anaerobic, nitrate-dependent oxidation of pyrite nanoparticles by *Thiobacillus denitrificans*. *Environ. Sci. Technol.* 46, 2095–2101. <https://doi.org/10.1021/es2022329>; pmid: 22142180.
- Brantley, S.L., Holleran, M.E., Jin, L., Bazilevskaya, E., 2013. Probing deep weathering in the Shale Hills Critical Zone Observatory, Pennsylvania (USA): the hypothesis of nested chemical reaction fronts in the subsurface. *Earth Surf. Proc. Landforms* 38, 1280–1298.
- Brenot, A., Baran, N., Petelet-Giraud, E., Négrel, P., 2008. Interaction between different water bodies in a small catchment in the Paris basin (Bréville, France): Tracing of multiple Sr sources through Sr isotopes coupled with Mg/Sr and Ca/Sr ratios. *App. Geochem.* 23, 58–75. <https://doi.org/10.1016/j.apgeochem.2007.09.006>.
- Bromley, J., Edmunds, W.M., Fellman, E., Brouwer, J., Gaze, S.R., Sudlow, J., Taupin, J.D., 1997. Estimation of rainfall inputs and direct recharge to the deep unsaturated zone of southern Niger using the chloride profile method. *J. Hydrol.* 188–189, 139–154.
- Cherchali, M.E.H., Liégeois, J.P., Mesbah, M., Daas, N., Amrous, K., Ouarezki, S.A., 2022. Central Hoggar groundwaters and the role of shear zones: ⁸⁷Sr/⁸⁶Sr, δ¹⁸O, δ²H and ¹⁴C isotopes, geochemistry and water-rock interactions. *App. Geochem.* 137, 105179. Cloutier, V., et al., 2008. Multivariate statistical analysis of geochemical data as indicative of the hydrogeochemical evolution of groundwater in a sedimentary rock aquifer system. *J. Hydrol.* 353, 294–313. <https://doi.org/10.1016/j.jhydrol.2008.02.015>.
- Cloutier, V., Lefebvre, R., Savard, M.M., Therrien, R., 2010. Desalination of a sedimentary rock aquifer system invaded by Pleistocene Champlain Sea water and processes controlling groundwater geochemistry. *Environm. Earth Sci.* 59, 977–994.
- Debure, M., Tournassat, C., Lerouge, C., Madé, B., Robinet, J.-C., Fernández, A.M., Grangeon, S., 2018. Retention of arsenic, chromium and boron on an outcropping clay-rich rock formation (the Tégulines Clay, eastern France). *Sci. Tot. Environ.* 642, 216–229.
- Debure, M., Grangeon, S., Robinet, J.-C., Made, B., Fernández, A., Lerouge, C., 2020. Influence of soil redox state on mercury sorption and reduction capacity. *Sci. Tot. Environ.* 707, 136069.
- Demonterova, E.I., Ivanov, A.V., Sklyarov, E.V., Pashkova, G.V., Klementiev, A.M., Tyagun, M.L., Vanin, V.A., Vologina, E.G., Yakhnenko, A.S., Yakhnenko, M.S., Kozyreva, E.A., 2022. ⁸⁷Sr/⁸⁶Sr of Lake Baikal: Evidence for rapid homogenization of water. *App. Geochem.* 144, 105420.
- Desaulniers, D.E., Cherry, J.A., Fritz, P., 1981. Origin, age and movement of pore water in argillaceous Quaternary deposits at four sites in southwestern Ontario. *J. Hydrol.* 50, 231–257.
- Ferguson, G., Cuthbert, M.O., Befus, K., Gleeson, T., McIntosh, J.C., 2020. Rethinking groundwater age. *Nat. Geosci.* 13, 592–594.
- Fernández, A.M., Sánchez-Ledesma, D.M., Tournassat, C., Melón, A., Gaucher, E.C., Astudillo, J., Vinsot, A., 2014. Applying the squeezing technique to highly consolidated clayrocks for pore water characterisation: lessons learned from experiments at the Mont Terri Rock Laboratory. *Appl. Geochem.* 49, 2–21.
- Z. Gao J. Liu J. Feng M. Wang G. Wu Hydrogeochemical Characteristics and the Suitability of Groundwater in the Alluvial-Diluvial Plain of Southwest Shandong Province China. *Water* 11 2019 - 10.3390/w11081577.
- Gaucher, É.C., Blanc, P., Bardot, F., Braibant, G., Buschaert, S., Crouzet, C., Gautier, A., Girard, J.-P., Jacquot, E., Lassin, A., Negrel, G., Tournassat, C., Vinsot, A., Altmann, S., 2006. Modelling the porewater chemistry of the Callovian-Oxfordian formation at a regional scale. *CR Geosci.* 338, 917–930.
- Girard, J.-P., Fléhoc, C., Gaucher, E., 2005. Stable isotope composition of CO₂ outgassed from cores of argillites: a simple method to constrain δ¹⁸O of porewater and δ¹³C of dissolved carbon in mudrocks. *Appl. Geochem.* 20, 713–725.
- Hadi, J., Tournassat, C., Lerouge, C., 2016. Pitfalls in using the hexaamminecobalt method for cation exchange capacity measurements on clay minerals and clay-rocks: Redox interferences between the cationic dye and the sample. *Appl. Clay Sci.* 119, 393–400.
- Hatrival, J.N., Menillet, F., 2002. French geological map 1/50 000 (n° 299). Brienne-le-Château. Notice explicative, Orléans, BRGM, p. 82.
- Hendry, M.J., Kelln, C.J., Wassenaar, L.I., Shaw, J., 2004. Characterizing the hydrogeology of a complex clay-rich aquitard system using detailed vertical profiles of the stable isotopes of water. *J. Hydrol.* 293, 47–56.
- Hendry, M.J., Wassenaar, L.I., 2000. Controls on the distribution of major ions in pore waters of a thick surficial aquitard. *Water Resour. Res.* 36, 503–513.
- Jankowski, J., Acworth, R.L., 1997. Impact of Debris-Flow Deposits on Hydrogeochemical Processes and the Development of Dryland Salinity in the Yass River Catchment, New South Wales, Australia. *Hydrogeol. J.* 5, 71–88.
- Jin, L., Brantley, S.L., 2011. Soil chemistry and shale weathering on a hillslope influenced by convergent hydrologic flow regime at the Susquehanna/Shale Hills Critical Zone Observatory. *App. Geochem.* 26, S51–S56.
- Jin, L., Ravella, R., Ketchum, B., Bierman, P.R., Heaney, P., White, T., Brantley, S.L., 2010. Mineral weathering and elemental transport during hillslope evolution at the Susquehanna/Shale Hills Critical Zone Observatory. *Geochim. Cosmochim. Acta* 74, 3669–3691.
- Jin, L., Mathur, R., Rother, G., Cole, D., Bazilevskaya, E., Williams, J., Carone, A., Brantley, S., 2013. Evolution of porosity and geochemistry in Marcellus Formation black shale during weathering. *Chem. Geol.* 356, 50–63.
- Jones, C.E., Jenkyns, H.C., 2001. Seawater strontium isotopes, oceanic anoxic events, and seafloor hydrothermal activity in the Jurassic and Cretaceous. *Am. J. Sci.* 301, 112–149.
- Kumar, P.J., James, E.J., 2016. Identification of hydrogeochemical processes in the Coimbatore district, Tamil Nadu, India. *Hydrol. Sci.* 61, 719–731. <https://doi.org/10.1080/02626667.2015.1022551>.
- Lakshmanan, E., Kannan, R., Senthilkumar, M., 2003. Major ion chemistry and identification of hydrogeochemical processes of ground water in a part of Kancheepuram district, Tamil Nadu, India. *Environm. Geosci.* 10, 157–166. <https://doi.org/10.1306/eg100403011>.
- Le Meur, M., Boussafir, M., Le Milbeau, C., Debure, M., Claret, C., Robinet, J.C., Lerouge, C., 2021. Organic matter oxidation of the Tégulines Clay formation, (Paris Basin, France): Spatial Heterogeneities. *App. Geochem.* 134, 105093, ISSN 0883-2927, <https://doi.org/10.1016/j.apgeochem.2021.105093>.
- Lerouge, C., Robinet, J.-C., Debure, M., Tournassat, C., Bouchet, A., Fernandez, A.M., Flehoc, C., Guerrot, C., Kars, M., Lagroix, F., Landrein, P., Madé, B., Negrel, P., Wille, G., Claret, F., 2018. A deep alteration and oxidation profile in a shallow clay aquitard: Example of the Tégulines Clay, East Paris Basin, France. *Geofluids* 2018, 20.
- Lerouge, C., Debure, M., Henry, B., Fernandez, A.-M., Blessing, M., Proust, E., Madé, B., Robinet, J.-C., 2020. Origin of dissolved gas (CO₂, O₂, N₂, alkanes) in pore waters of a clay formation in the critical zone (Tégulines Clay, France). *App. Geochem.*, p. 104573.
- Li, L., Maher, K., Navarre-Sitchler, A., Druhan, J., Meile, C., Lawrence, C., Moore, J., Perdril, J., Sullivan, P., Thompson, A., Jin, L., Bolton, E.W., Brantley, S.L., Dietrich, W.E., Mayer, K.U., Steefel, C.I., Valocchi, A., Zachara, J., Kocar, B., McIntosh, J., Tutolo, B.M., Kumar, M., Sennenthal, E., Bao, C., Beisman, J., 2017. Expanding the

- role of reactive transport models in critical zone processes. *Earth Sci. Rev.* 165, 280–301.
- Li, P., Qian, H., Wu, J., Zhang, Y., Zhang, H., 2013. Major Ion Chemistry of Shallow Groundwater in the Dongsheng Coalfield, Ordos Basin, China. *Mine Water Environ.* 32, 195–206. <https://doi.org/10.1007/s10230-013-0234-8>.
- MacQuarrie, K.T., Mayer, K.U., 2005. Reactive transport modeling in fractured rock: a state-of-the-science review. *Earth Sci. Rev.* 72, 189–227.
- Maier, K., Steefel, C.I., DePaolo, D.J., Viani, B.E., 2006. The mineral dissolution rate conundrum: insights from reactive transport modeling of U isotopes and pore fluid chemistry in marine sediments. *Geochim. Cosmochim. Acta* 70, 337–363.
- Mayer, K.U., Alt-Epping, P., Jacques, D., Arora, B., Steefel, C.I., 2015. Benchmark problems for reactive transport modeling of the generation and attenuation of acid rock drainage. *Comput. Geosci.* 19, 599–611.
- Mazurek, M., Alt-Epping, P., Gimi, T.h., Niklaus Waber, H., Bath, A., Gimmi, T.h., 2009. Natural tracer profiles across argillaceous formations: the Claytrac project. Organisation for Economic Co-Operation and Development Nuclear Energy Agency, Nuclear Energy Agency of the OECD (NEA).
- Mazurek, M., Alt-Epping, P., Bath, A., Gimmi, T., Niklaus Waber, H., Buschaert, S., Cannière, P.D., Craen, M.D., Gautschi, A., Savoye, S., Vinsot, A., Wemaere, I., Wouters, L., 2011. Natural tracer profiles across argillaceous formations. *App. Geochem.* 26, 1035–1064.
- Milesi, V.P., Debure, M., Marty, N.C., Capano, M., Jézéquel, D., Steefel, C., Rouchon, V., Albéric, P., Bard, E., Sarazin, G., Guyot, F., Virgone, A., Gaucher, E.C., Ader, M., 2020. Early diagenesis of lacustrine carbonates in volcanic settings: the role of magmatic CO₂ (Lake Dziani Dzaha, Mayotte, Indian Ocean). *ACS Earth Space Chem.* 4, 363–378.
- Pacheco, F.A.L., Alencôo, A.M.P., 2006. Role of fractures in weathering of solid rocks: narrowing the gap between laboratory and field weathering rates. *J. Hydrol.* 316, 248–265.
- Rajmohan, N., Elango, L., 2004. Identification and Evolution of Hydrogeochemical Processes in the Groundwater Environment in an Area of the Palar and Cheyyar River Basins, Southern India. *Environ. Geol.* 46, 47–61. <https://doi.org/10.1007/s00254-004-1012-5>.
- Remenda, V.H., Cherry, J.C., Edwards, T.W.D., 1994. Isotopic composition of old ground water from Lake Agassiz: Implications for late Pleistocene climate. *Sci.* 266, 1975–1978.
- Sajil Kumar, P.J., James, E.J., 2016. Identification of hydrogeochemical processes in the Coimbatore district, Tamil Nadu, India. *Hydrol. Sci. J.* 61, 719–731.
- Sebilo, M., Mayer, B., Nicolardot, B., Pinay, G., Mariotti, A., 2013. Long-term fate of nitrate fertilizer. *Proc. Natl. Acad. Sci.* 110, 18185–18189. <https://doi.org/10.1073/pnas.1305372110>.
- Subramani, T., Rajmohan, N., Elango, L., 2010. Groundwater geochemistry and identification of hydrogeochemical processes in a hard rock region, Southern India. *Environ. Monitor. Assess.* 162, 123–137.
- Sullivan, P.L., Ma, L., West, N., Jin, L., Karwan, D.L., Noireaux, J., Steinhofel, G., Gaines, K.P., Eissenstat, D.M., Gaillardet, J., Derry, L.A., Meek, K., Hynek, S., Brantley, S.L., 2016. CZ-tope at Susquehanna Shale Hills CZO: Synthesizing multiple isotope proxies to elucidate Critical Zone processes across timescales in a temperate forested landscape. *Chem. Geol.* 445, 103–119.
- Sun, J., Takahashi, Y., Strosnider, W.H.J., Kogure, T., Wang, B., Wu, P., Zhu, L., Dong, Z., 2021. Identification and quantification of contributions to karst groundwater using a triple stable isotope labeling and mass balance model. *Chemosphere* 263, 127946.
- Tremosa, J., Debure, M., Narayanasamy, S., Redon, P.O., Jacques, D., Claret, F., Robinet, J.C., 2020. Shale weathering: A lysimeter and modelling study for flow, transport, gas diffusion and reactivity assessment in the critical zone. *J. Hydrol.* 587, 124925.
- Tuttle, M.L.W., Breit, G.N., 2009. Weathering of the New Albany Shale, Kentucky, USA: I. Weathering zones defined by mineralogy and major-element composition. *App. Geochem.* 24, 1549–1564.
- Tuttle, M.L.W., Breit, G.N., Goldhaber, M.B., 2009. Weathering of the New Albany Shale, Kentucky: II. Redistribution of minor and trace elements. *App. Geochem.* 24, 1565–1578.
- Voinchet, P., Brulhet, J., Cojan, I., Bahain, J.J., Falguères, C., 2012. Datation ESR des terrasses alluviales pléistocènes de la vallée de l'Aube : premiers résultats. *Quat.* 26, 185–193. <https://doi.org/10.4000/qua.7376>.
- Ward, M.H., Jones, R., Brender, J.D., de Kok, T.M., Weyer, P.J., Nolan, B.T., Villanueva, C.M., Simone, G., van Breda, S.M., 2018. Drinking Water Nitrate and Human Health: An Updated Review. *Int. J. Environ. Res. Public Health.* 15, 1557. Published online 2018 Jul 23. doi: 10.3390/ijerph15071557.
- Wersin, P., Mazurek, M., Mäder, U.K., Gimmi, T., Rufer, D., Lerouge, C., Traber, D., 2016. Constraining porewater chemistry in a 250 m thick argillaceous rock sequence. *Chem. Geol.* 434, 43–61.